CSPBankability Project Report

Draft for an Appendix C – Solar Field Modeling

to the SolarPACES Guideline for Bankable STE Yield Assessment

Document prepared by the project CSPBankability funded by the German Federal Ministry Economic Affairs and Energy under contract No. 0325293.

Gefördert durch:

Bundesministerium für Wirtschaft und Energie

aufgrund eines Beschlusses des Deutschen Bundestages

Document properties

Title	CSPBankability Project Report: Draft for an Appendix C – Solar Field Modeling to the SolarPACES Guideline for Bankable STE Yield Assessment
Editor	Tobias Hirsch (DLR)
Author	Jürgen Dersch, Stefano Giuliano (DLR)
Contributing authors	Enver Yildiz (Fichtner) Camille Bachelier (Frenell) Simon Lude Olaf Goebel (University of Applied Science Hamm-Lippstadt) Norbert Schmidt (DNV-GL) Michael Puppe (DLR) Christoph Rau (IATech)
Date	January 9, 2017

Index of contents

C. Modelling of “Solar field SF”

The solar field collects energy delivered by sun beams, converts it into sensible and/or latent heat of a fluid, and transports the heat via this fluid to the power block and/or to the thermal storage. Depending on individual CSP technologies solar field look different which in turn leads to specific modelling approaches. This appendix starts with a general approach and then turns to the specific ones with models for each physical effect with significant impact on the annual yield. In the current context “significant” means that neglecting the individual effect would change the annual electrical yield by approximately 1 % or more.

C.1. General modeling approach

Although the solar field technologies differ some fundamentals are very similar and allow to define generic approaches applicable to all of them. This section introduces some general aspects that are used by the technology-specific chapters that follow. These are:

- An generic equation for describing steady-state performance
- The definition of the aperture area
- Interface and monitoring variables.

C.1.1. Generic modeling approach

The general quasi dynamic equation for the thermal power delivered by the solar field of CSP systems may be written as:

$$\dot{Q}^{\mathrm{SF}} = \dot{Q}_{\mathrm{avail}} - \sum \dot{Q}_{\mathrm{loss}} + \sum \dot{Q}_{\mathrm{gain}} - \dot{Q}_{trans} \qquad \text{(C.1)}$$

It consists of the available radiant solar power reduced by thermal losses and increased by heat gains from other sources (e.g. the power of solar field pumps but also from trace heating if applicable) and a transient correction term.
According to the general energy chain, the available radiant solar power reduced by all optical losses is leading to the absorbed thermal power.

$$\dot{Q}_{\mathrm{abs}} = \eta_{opt}\, \dot{Q}_{avail} \qquad \text{(C.2)}$$

The absorbed thermal power for many CSP systems consists of 2 parts: the irradiance collected by the reflectors and redirected to the receiver and the irradiance which hits the receiver directly. The latter one is typically much smaller than the first one since the reflective area is much larger than the receiver area.

Following formula allows for determination of the absorbed thermal power:

$$\dot{Q}_{\mathrm{abs}} = \eta_{\mathrm{phi}}\ \eta_{\mathrm{shad}}\ \eta_{\mathrm{refl,0}}\ \eta_{\mathrm{reflclean}}\ \eta_{\mathrm{block}}\ \eta_{\mathrm{atten}} \quad \text{(C.3)}$$
$$\eta_{\mathrm{inter}}\ \eta_{\mathrm{recclean}}\ \eta_{\mathrm{trans}}\ \eta_{\mathrm{abs}}\ \eta_{\mathrm{avail}}\ f_{\mathrm{focA}}\ A_{\mathrm{nom*}}\ G_{\mathrm{bn}}$$
$$+ A_{\mathrm{rec}}\left(\eta_{\mathrm{phi,rec}} G_{\mathrm{bn}} + G_{\mathrm{d}}\right) \eta_{\mathrm{recclean}}\ \eta_{\mathrm{trans}}\ \eta_{\mathrm{abs}}$$

With:

$\dot{Q}_{\mathrm{abs}}$	Absorbed thermal power in kW
η_{phi}	Incidence angle efficiency including all losses caused by non-perpendicular sun rays into the aperture plane, dimensionless
η_{shad}	Shading efficiency, dimensionless
$\eta_{\mathrm{refl,0}}$	Clean reflector efficiency, dimensionless
$\eta_{\mathrm{reflclean}}$	Reflector cleanliness factor, dimensionless
η_{block}	Blocking efficiency, dimensionless
η_{atten}	Atmospheric attenuation efficiency, dimensionless
η_{inter}	Intercept factor, dimensionless
η_{recclean}	Receiver cleanliness factor, dimensionless
η_{trans}	Transmission through receiver glass cover (if any), dimensionless
η_{abs}	Receiver absorptance dimensionless
η_{avail}	Solar field availability, dimensionless
f_{focA}	Focusing factor, fraction of the actual aperture area in operation over the total nominal aperture area, or fraction of the actual intercept efficiency over the nominal intercept efficiency
$A_{\mathrm{nom*}}$	Nominal aperture area without receiver area in m²
A_{rec}	Receiver area in m²
G_{bn}	Direct normal solar irradiance in W/m²
G_{d}	Diffuse irradiance in W/m²

The focusing factor f_{focA} represents the fraction of the solar field aperture area actually in operation or the actual intercept efficiency over the nominal intercept efficiency, depending on the applied control strategy. During certain time periods the solar field must be partially defocused because the power block runs at maximal load and the thermal storage is fully charged. In order to prevent overheating some of the installed mirrors are turned in out of focus to adapt the actual solar field output to the desired output. For parabolic trough plants another control strategy is often used: instead of turning whole collectors or loops in a position where they do not collect any solar irradiance, they are just turned out of the ideal tracking position by a small angle in a way that a certain fraction of the reflected sun beams are not hitting the absorber tube. This control strategy enables a smoother adaption of the solar field output to the requirements than the one mentioned before. In terms of Eq. (C.3) this second control strategy means that the intercept efficiency of the system is reduced.

Due to nonlinearities, f_{focA} is not identical to the fraction of thermal power delivered by the solar field divided by the maximal possible thermal power of the solar field in the relevant period. Thus, an iterative procedure is necessary to calculate this factor (see system simulation in Appendix H). The maximal possible thermal power of the solar field can be calculated by setting the factor f_{focA} to 1.0.

C.1.2. Definition of the relevant aperture area

The equations in this chapter are typically written in terms of the nominal aperture area of the parabolic trough collectors. This reference value has been chosen instead of the net or gross aperture area because a common definition of these figures is still not available. As long as there is no common understanding about the definition, each supplier defines the aperture area of his collector as he wants. Therefore in this guideline the nominal aperture area is used, which is the one defined by the supplier. It is very important to use all other parameters (e.g. peak optical efficiency and specific cost figures) in a way consistent with the nominal aperture area. See also the definitions for aperture areas in Appendix T.

C.1.3. Interface and result variables for the solar field sub-system

The sub-system systematics as explained in Appendix A describes the way the solar field model interacts with the rest of the plant model. Through the interface variable definition a unique set of variables is defined that are used to exchange information between the solar field sub-system and the system level. In addition to the interface variables, reporting variables are defined. The reporting variables are not needed during the simulation but provide information from the sub-system calculation that is required for evaluating characteristic figures on system level. Since the principle functionality of the solar field is similar at least when it comes to the interfaces a set of interface and reporting variables is defined in Table C-1. The first block holds the elementary interface variables as defined in Appendix A which are valid for all technologies. The list is completed by technology specific variables like the cosine of the incident angle for line focusing systems. Some reporting variables can only be evaluated if the underlying modeling approach breaks down the energy chain on an effect level. Black box type modeling approaches will have integrated all effects but might not foresee to extract intermediate results.

Table C-1: Interface (I) and reporting (R) variables valid for solar field technologies (*indicates variables that might not be available for all modeling approaches)

Type	Name	Symbol	Comment
I	Inlet temperature	$\boldsymbol{T}_{\mathrm{in}}^{\mathrm{SF}}$	
I	Outlet temperature	$\boldsymbol{T}_{\mathrm{out}}^{\mathrm{SF}}$	
I	Inlet pressure	$\boldsymbol{p}_{\mathrm{in}}^{\mathrm{SF}}$	
I	Outlet pressure	$\boldsymbol{p}_{\mathrm{out}}^{\mathrm{SF}}$	
I	mass flow	$\dot{\boldsymbol{m}}^{\mathrm{SF}}$	
I	Ambient temperature	T_{amb}	
I	Direct normal irradiance	G_{bn}	
I	Wind direction/speed	$\boldsymbol{v}_{\mathbf{wind}}$, $\boldsymbol{\gamma}_{\mathrm{wind}}$	
I	Auxiliary electrical demand	$\boldsymbol{P}_{\mathrm{aux}}^{\mathrm{SF}}$	
I	Acceptable minimum/maximum mass flow	$\dot{\boldsymbol{m}}_{\mathrm{min/max}}^{\mathrm{SF}}$	
I	Set point outlet temperature	$\boldsymbol{T}_{\mathrm{out,set}}^{\mathrm{SF}}$	
I	Set point mass flow	$\dot{\boldsymbol{m}}_{\mathrm{set}}^{\mathrm{SF}}$	
R	Solar field thermal power	$\dot{\boldsymbol{Q}}^{\mathrm{SF}}$	
R	Available radiant solar power	$\dot{\boldsymbol{Q}}_{\mathrm{avail}}$	
R	Absorbed power	$\dot{\boldsymbol{Q}}_{\mathrm{abs}}$	
R	Percentage of field operational*	$\boldsymbol{f}_{\mathrm{foc,A}}$	
R	Maximum load defocussing power*	$\dot{\boldsymbol{Q}}_{\mathrm{defoc,max}}$	
R	Minimum load defocussing power*	$\dot{\boldsymbol{Q}}_{\mathrm{defoc,min}}$	
R	Receiver heat loss power*	$\dot{\boldsymbol{Q}}_{\mathrm{loss,rec}}$	
R	Solar field piping thermal loss power*	$\dot{\boldsymbol{Q}}_{\mathrm{loss,pipe}}$	
R	Header piping thermal loss power*	$\dot{\boldsymbol{Q}}_{\mathrm{loss,head}}$	
R	HTF equipment thermal loss power*	$\dot{\boldsymbol{Q}}_{\mathrm{loss,equ}}$	

Table C-2: Special interface (I) and reporting (R) variables for line focusing solar fields
(*indicates variables that might not be available for all modeling approaches)

Type	Name	Symbol	Comment
R	Projected radiant solar power	$\dot{Q}_{\mathrm{proj}}$	
R	Incidence angle modifier	K	

C.2. Line focusing solar fields

All the different solar field technologies based on line focusing concentrators can be modelled more or less similar. Parabolic trough systems with synthetic oil as heat transfer medium are described in detail in the first chapter. Most of the approaches can be transferred to parabolic trough configurations with other heat transfer media like e.g. molten salt as well as to other concentrator technologies like Linear Fresnel. The structure of this document uses the parabolic trough with oil as reference case. Modifications required for other technologies are described in subsequent chapters (provided in the next version of the guideline).

C.2.1. Parabolic trough field with oil

At present, parabolic trough plants with single heat transfer fluid represent the most frequently used technology in CSP. The majority of them use an eutectic mixture of diphenyl oxide (DPO) and biphenyl (BP). The best known products are Therminol® VP-1, Dowtherm® A or Diphyl®. This heat transfer fluid (HTF) is liquid between 12 °C and the upper operating temperature of 400 °C, provided that the system is pressurized and the pressure is always above the vapor pressure (10.9 bar at 400 °C). Above 400 °C the decomposition rate of DPO/BP is rapidly increasing and, therefore, 400 °C is the upper bulk temperature limit for these plants. Film temperature in the boundary layer of externally heated receiver tubes may be higher. According to the VP-1 datasheet the maximum film temperature is 430 °C.

The modelling approaches given in this chapter are mainly developed for this DPO/BP fluid but they are in principle valid also for other single phase fluids, such as molten salts for example. The current version of this document deals with DPO/BP as HTF.

The first chapter introduces the principle modeling approach for the parabolic trough technology operated with single phase heat transfer media. Subsequent chapters provide detailed modeling approaches for the optical losses, thermal losses, pressure loss, and electric consumption. Additional chapters afterwards describe how to model transient behavior, load limitations, and night operation. The chapter ends with a number of plausibility checks as support for the user.

C.2.1.1. Specific modeling approach for this technology

Parabolic troughs are arranged in loops which are interconnected by so called header and runner pipes. Headers and runners are considered jointly in the energy balance below. The whole solar field might be divided into subfields. Typically, the simulation is done for one representative loop and the total power is calculated by multiplying the output of this representative loop by the total number of loops. The figure below depicts exemplarily the layout of a parabolic trough CSP plant.

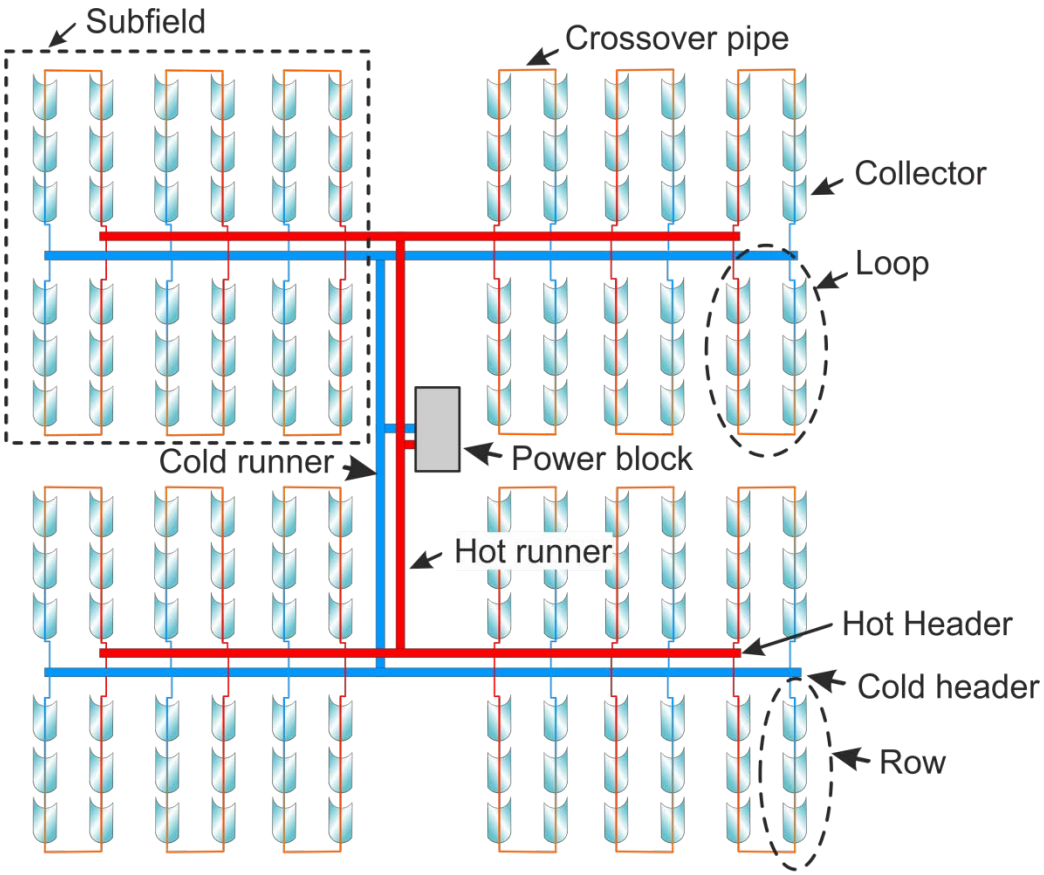

Figure C-1: Typical layout of a parabolic trough CSP plant

The solar field output at steady state conditions can be calculated by the following equation:

$$\dot{Q}_{\text{steady}}^{\text{SF}} = \dot{Q}_{\text{abs}} - \dot{Q}_{\text{loss,rec}} - \dot{Q}_{\text{loss,pipe}} - \dot{Q}_{\text{loss,head}} + \dot{Q}_{\Delta\text{p}} \qquad \text{(C.4)}$$

Due to practical considerations, the diffusive irradiation term in (C.3) is not used for parabolic trough systems and the equation for the absorbed power is reduced to:

$$\dot{Q}_{\text{abs}} = \eta_{\text{phi}}\ \eta_{\text{shad}}\ \eta_{\text{refl,0}}\ \eta_{\text{clean}}\ \eta_{\text{block}}\ \eta_{\text{atten}}\ \eta_{\text{inter}}\ \eta_{\text{trans}}\ \eta_{\text{abs}}\eta_{\text{avail}}^{\text{SF}}\ f_{\text{foc,A}}\ A_{\text{nom}}\ G_{\text{bn}} \qquad \text{(C.5)}$$

Nevertheless, the irradiance absorbed directly by the receiver is not neglected in (C.5) since the nominal aperture area in this equation is typically defined in a manner that the receiver area is included, in contrast to $A_{\mathrm{nom}*}$ used in Eq. (C.3). This might be considered as a slightly conservative approach since the diffuse irradiance onto the receiver is neglected and the direct irradiance on it is reduced by the reflectivity of the mirrors although the irradiance is not redirected by the mirrors. The cleanliness is considered by a single effective value.
Furthermore, several effects from Eq. (C.3) are merged into the peak optical efficiency as shown in Eq. (C.6). This peak optical efficiency is defined for a single collector, a complete device of around 100 m in length or more for usual commercial industrial scale collectors, which can be tracked as one unit.

$$\eta_{\mathrm{opt},0} = \eta_{\mathrm{refl},0}\ \eta_{\mathrm{block}}\ \eta_{\mathrm{atten}}\ \eta_{\mathrm{inter}}\ \eta_{\mathrm{trans}}\ \eta_{\mathrm{abs}} \qquad \text{(C.6)}$$

The optical efficiency is measured by manufacturers or laboratories and given on the collector data sheets. For the utilization of the relevant value in terms of a model, it is important that optical efficiency and corresponding nominal aperture area are specified together since the value of the optical efficiency depends on the actual definition of aperture area. The same statement is valid for specific costs based on the aperture area. The following table shows 2 different aperture areas for Eurotrough SKAL-ET collectors and the corresponding optical efficiencies. The nominal aperture area of 817.5 m² and corresponding optical efficiency of 78 % have been published by [Herrmann 2004]. If the gross aperture area calculated from the collector outer dimensions is used in the equations for the calculation of the solar field output instead of the nominal aperture, the optical efficiency value must be reduced by 3.6 % points in order to yield the correct absorbed power. The example shows that the aperture area definition and the corresponding performance data need to be carefully checked for consistence before they are used for the yield calculation.

Table C-3: Two coupled pairs of aperture area and optical efficiency for the Eurotrough collector

Parameter	**value**	**unit**
Nominal aperture area	817.5	m²
Nominal optical efficiency	78	%
Collector length	148.5	m
Aperture width	5.77	m
Gross aperture area	856.8	m²
Gross optical efficiency	74.4	%

The optical efficiency is only valid for a certain combination of reflector and receiver and must be determined for each collector. Design modifications of the collector or utilization of other receiver types will lead to other optical efficiency of the system.

Table C-4: Reference value for the optical efficiency of the Eurotrough collector and typical range for the optical efficiency of parabolic trough collectors

Reference value	Default value	Range	Uncertainty	unit
Nominal optical efficiency	0.78	0.65 … 0.82	t.b.d.	-
Nominal aperture area	817.5	n.a.	n.a.	m²

The efficiency term used for losses caused by non-perpendicular incoming sun rays into the aperture plane is expressed by cosine losses, incidence angle modifier K, and end losses.

$$\eta_{\mathrm{phi}} = \cos(\theta_{\mathrm{i}}) \cdot K(\theta_{\mathrm{i}}) \cdot \eta_{\mathrm{endloss}} \quad \text{(C.7)}$$

Typically, the solar field is made of many identical collectors, thus the total absorbed thermal power of the solar field, a single loop or a single collector may be calculated by:

$$\dot{Q}_{\mathrm{abs}} = cos(\theta_{\mathrm{i}})\ K(\theta_{\mathrm{i}})\, \eta_{\mathrm{endloss}}\, \eta_{\mathrm{opt,0}}\, \eta_{\mathrm{shad}}\, \eta_{\mathrm{clean}}\, \eta_{\mathrm{avail}}\, f_{\mathrm{focA}}\, A_{\mathrm{nom}}\ G_{\mathrm{bn}} \quad \text{(C.8)}$$

Or, in terms of the projected direct irradiance:

$$\dot{Q}_{\mathrm{abs}} = K(\theta_{\mathrm{i}})\, \eta_{\mathrm{endloss}}\, \eta_{\mathrm{opt,0}}\, \eta_{\mathrm{shad}}\, \eta_{\mathrm{clean}}\, \eta_{\mathrm{avail}}\, f_{\mathrm{focA}}\, A_{\mathrm{nom}}\ G_{\mathrm{pr}} \quad \text{(C.9)}$$

With the appropriate total area A_{nom} of the whole solar field, of one loop or of one collector, respectively. The proposal in this handbook is to calculate the absorbed heat for a single representative loop since many heat loss effects can easily be calculated for a single loop.
Should the solar field consist of different collector types or different loop arrangements, these subfields may be calculated separately and results for the total field may be generated by summing up the individual results.
For parabolic trough solar fields, defocusing can be done for whole loops or by defocusing some or all collectors in each loop by a small fraction and reducing the intercept efficiency by this measure. The second approach allows for smoother operation and is considered in this model. Therefore, the factor f_{focA} is valid for the whole solar field as well as for single loops.

Incidence angle for parabolic troughs

The incidence angle of the sun rays onto the aperture is of particular importance for parabolic troughs and other single axis tracking CSP systems.

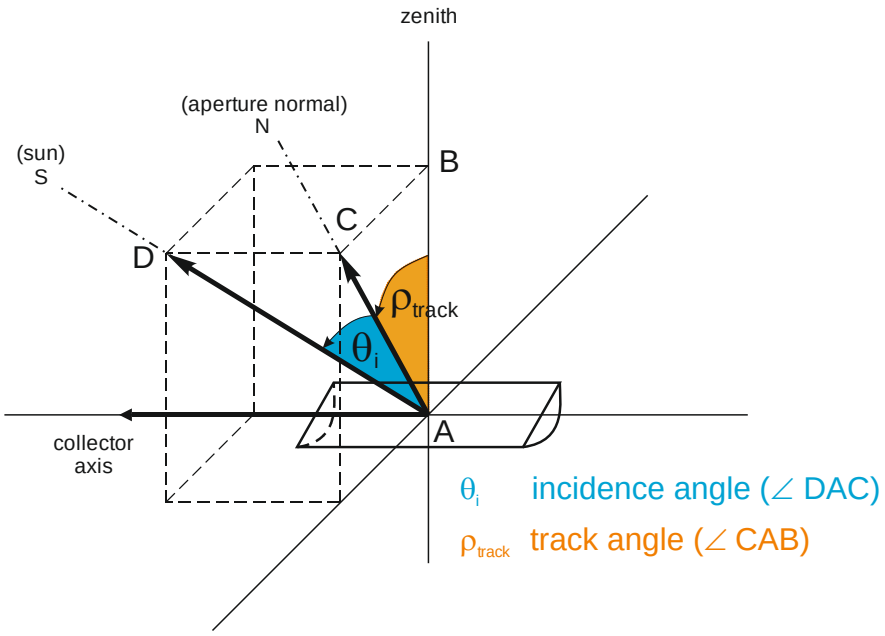

Figure C-2: Incidence angle and track angle for a parabolic trough

The incidence angle of an arbitrarily oriented parabolic trough collector may be calculated from [Stine 1985]:

$$\cos(\theta_i) = \sqrt{1 - [\cos(\alpha_S - \beta_A) - \cos(\beta_A) \cdot \cos(\alpha_S) \cdot (1 - \cos(\gamma_S - \gamma_A))]^2} \qquad \text{(C.10)}$$

The calculation of solar azimuth angle γ_S and solar altitude angle α_S is explained in Appendix J "Meteorological Conditions".

The collector track angle is determined by:

$$\tan(\rho_{track}) = \frac{\cos(\alpha_S) \cdot \sin(\gamma_S - \gamma_A)}{\sin(\alpha_S - \beta_A) + \sin(\beta_A) \cdot \cos(\alpha_S) \cdot [1 - \cos(\gamma_S - \gamma_A)]} \qquad \text{(C.11)}$$

With

θ_i	incidence angle in degrees
ρ_{track}	collector track angle in degrees
γ_S	solar azimuth angle in degrees
α_S	solar altitude angle in degrees
γ_A	collector axis azimuth angle in degrees
β_A	collector axis tilt angle in degrees

See Appendix T.3.2 for the definition of solar and collector angles.

Users should take particular care of the time of reference used in the annual performance calculation and in the meteorological dataset. Meteorological datasets derived from satellite data often use coordinated universal time (UTC) since satellite images typically cover several time zones. Annual performance models in contrast often use local time at site since this allows for direct comparison of the generated electricity with demand profiles or time dependent tariffs.
The situation gets even more complicated when daylight saving time is observed during summer months at the specific site. In this case, a meteorological dataset based on daylight savings time has missing or surplus values for those hours when the local time is shifted to daylight saving time or vice versa. The recommendation is to stay with UTC or local (winter time) for the technical simulations and consider the time shift in the load or tariff matrix.
Furthermore, it is important to check the definition of the time stamp used in the meteorological data file. Time stamp means that the meteorological data file and also the model output will use a time indication which actually stands for a time period. Therefore, at least three interpretations are possible for the relation between time stamp and associated period: the time stamp represents the preceding period, the following period or the center of the period. In this handbook, we assume that a time stamp like 12:00 in a file with hourly resolution means that the data represents the mean values of DNI, ambient temperature, ambient humidity, etc. in the preceding time step. Therefore, the corresponding mean sun position is that of 11:30!
This is valid for most hours of the day except for the time periods of sunrise and sunset. The sun position in the middle of those hours might be below horizon and therefore not representative for the yield calculation. Instead, the sun position for these hours should be calculated for the center of the time interval between sunrise and the next time stamp in the morning and between the previous time stamp and sunset in the evening. For datasets with higher temporal resolution than one hour this rule can be applied accordingly.

Example for the correction of DNI and sun position for hourly time steps

In case of large time steps like 1 hour for the simulation it might be necessary to pay particular attention to the time steps of sunrise and sunset. Sun position and mean DNI values should be checked and corrected if necessary.
Figure C-3 shows an example for the correction of DNI and sun position in case of large time steps like 1 hour. Sunrise is just after 6:30 and the 10 minutes dataset shows 1, 99 and 295 W/m² for the first three time steps after sunrise. Mean DNI using hourly resolution would result in 66 W/m² for this first hour. For the simulation it makes a difference whether the mean values (averaged over one hour) of DNI and sun position are used or corrected values for DNI and sun position that take into account the sunrise event. Let us assume that only the information of the blue columns (mean hourly values) in Figure C-3 is available, together with the time of sunrise. The 10 min data in this figure are just shown for demonstration purposes. First, the corrected solar position to be used for the performance calculation needs to be calculated based on the time of sunrise for 6:45. In the next step, the hourly averaged DNI of 66 W/m^2 needs to be corrected for the time interval after sunrise (66 W/m²*60 min/29 min = 137 W/m²). The difference between the original 66 W/m^2 and the corrected 137 W/m^2

is significant. Prior to the application of this kind of correction, it must be checked whether it was not already done during the compilation of the meteorological dataset (see Appendix J) in order to avoid a double correction!

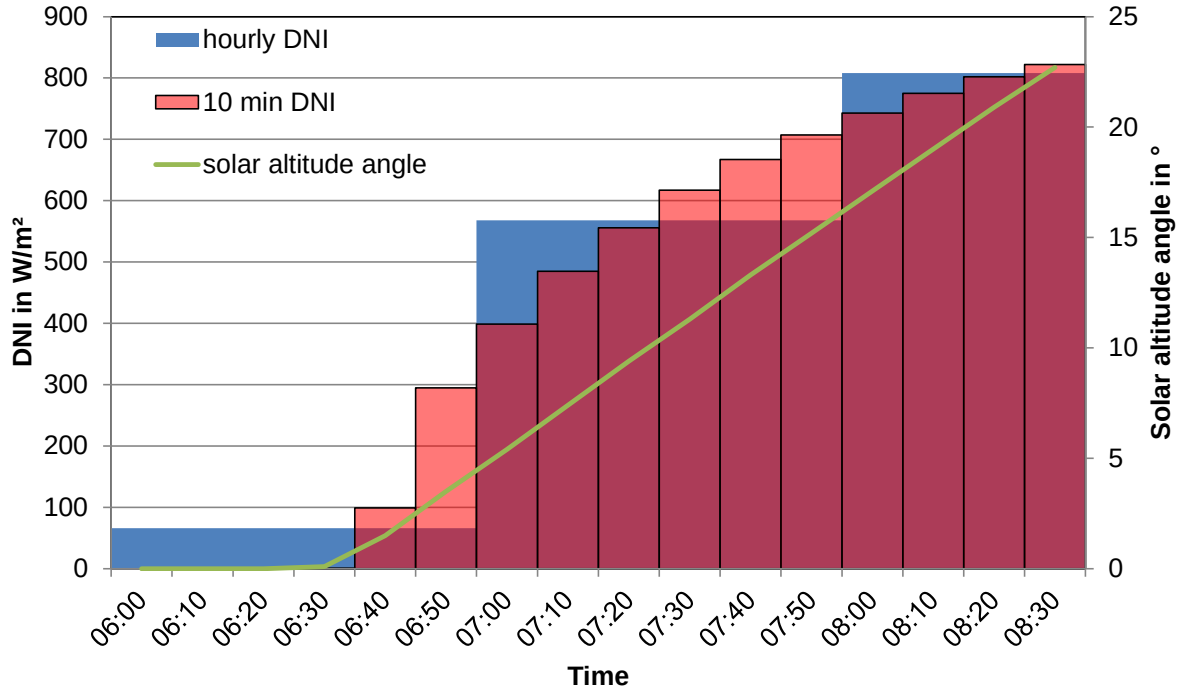

Figure C-3: Mean DNI for different temporal resolutions and solar altitude angle in early morning hours

However, when 10 minutes are used as time step for the whole simulation, it will be sufficient to use always the sun position at the middle of the time interval together with the beam radiation from the meteorological data file. The error of this simplification is negligible. For low solar altitude angles (< 10°) row-to-row shading as well as high atmospheric attenuation reduce the usable direct irradiance. It is recommended to carry out a simulation also for those time steps and check whether a positive heat gain is possible or not. Operators in existing plants may use a certain threshold solar altitude angle instead of such a calculation. However, such threshold angle is difficult to determine in a common way. Thus, having the model available it will be easier to determine whether there is a net heat gain from the solar field or not.

Impact of temporal resolutions on annual performance results

The required temporal resolution for annual performance models is a matter of discussion since several years. This guideline recommends the utilization of 10 minutes time steps since high quality meteorological date is typically available with this resolution, modern computers are fast enough and the model formulation is simpler, particularly for those time steps with startup operation or when certain limits are reached (e.g. storage is totally charged or discharged). When hourly time steps are

used, these particular time periods need to be further split up. When using 10 minutes as temporal resolution, the impact of a single time step is small enough to assume just a single operating mode and omit further splitting.
The TMY datasets for the PSA (Spain) have been used to investigate the impact of different time steps. The example was an annual performance calculation for a 50 MWe parabolic trough plant with 7 hours of thermal storage. A TMY data file with 10 minutes resolution was available as well as a data file with 60 minutes resolution representing the mean values of the 10 minutes data file. Table C-5 show the results of 3 simulations: 10 minutes simulation time step using the 10 minutes meteorological dataset, hourly simulation using the hourly mean meteorological dataset and 10 minutes simulation using the hourly meteorological data. For the latter one, every 6 individual values within one hour are set to the same mean value of the respective hour.
Table C-5 shows that the differences in annual electrical net electrical output are quite small and in this case the 10 minutes simulation together with 60 minutes meteorological data results in even higher deviation than the 60 minutes simulation with 60 minutes meteorological data. This is of course only one example but previous investigations showed similar trends [Dersch 2012]. Nevertheless, this handbook recommends the utilization of 10 minutes time steps due to the reasons explained above.

Table C-5: Impact of temporal resolution on annual electrical output

Simulation time step	**10 min**	**60 min**	**10 min**	**Unit**
Meteo data time step	**10 min**	**60 min**	**60 min**	
E_{net}	151965	152508	150935	MWh
$E_{net,rel}$	1.000	1.004	0.993	-

C.2.1.2. Optical losses

A solar collector has several optical loss effects that are described in the following paragraphs.

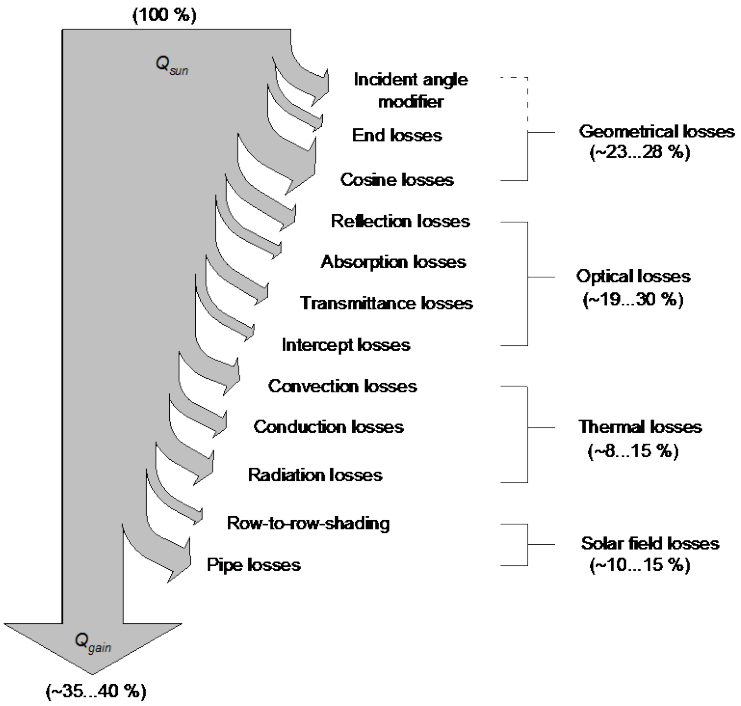

Figure C-4: Sankey diagram showing the energy chain from solar resource to heat delivered by the solar field

Cosine losses

When the collector aperture is not perpendicular to the sun rays, the projected aperture area is reduced. Parabolic trough collectors are tracked in a manner that sun beams are within the plane defined by the collector aperture normal and the collector axis. Since parabolic trough collectors are single axis tracking collectors there is a certain angle between sun vector and aperture normal vector for most sun positions (the incidence angle). Thus, the apparent aperture area as seen from the sun is reduced.

The reduced aperture area depends on the cosine of the incidence angle which is the reason for calling these losses cosine losses.

$$\eta_{\cos} = cos(\theta_{\mathrm{i}}) = \frac{G_{\mathrm{pr}}}{G_{\mathrm{bn}}} \tag{C.12}$$

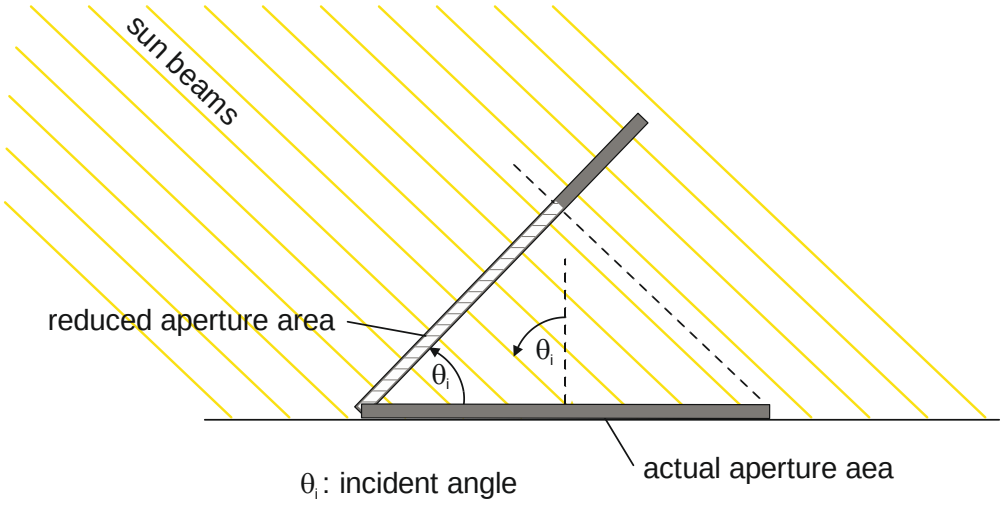

Figure C-5: Effective aperture reduction caused by non-perpendicular sun rays onto the aperture (cosine losses)

Row-to row shading

If there are no mountains or other huge structures close to the solar field, the major shading mechanism is the so called row-to-row shading caused by other parabolic troughs of the neighbor row in the solar field. Shading caused by nearby buildings or mountains etc. is considered in the next paragraph.

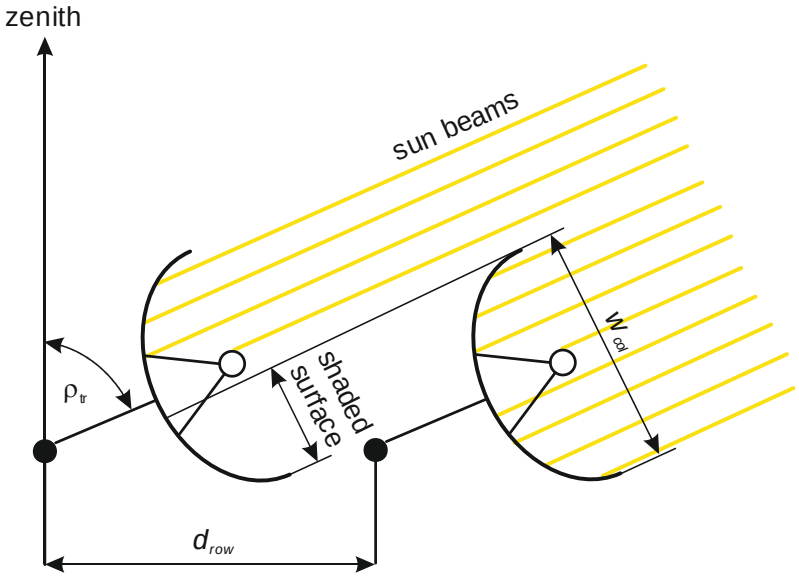

Figure C-6: Row-to-row shading in a parabolic trough solar field

Row-to-row shading is a geometrical effect and can be calculated from:

$$\eta_{\text{shad,row}} = \frac{d_{row}\, cos(\rho_{tr})}{w_{col}} \quad \text{for} \quad 0 \leq \frac{d_{row}\, cos(\rho_{tr})}{w_{col}} \leq 1 \tag{C.13}$$

$$\eta_{\text{shad,row}} = 0 \quad \text{for} \quad \frac{d_{row}\, cos(\rho_{tr})}{w_{col}} < 0$$

$$\eta_{\text{shad,row}} = 1 \quad \text{for} \quad \frac{d_{row}\, cos(\rho_{tr})}{w_{col}} > 1$$

With:

w_{col} collector aperture width in m

d_{row} row-to-row distance in m

Row-to-row shading has only a significant impact for low solar altitude angles. Most of the existing large parabolic trough solar fields use a row distance of about 3 aperture widths and south-north oriented collector axes. For these configurations the annual row-to-row shading losses are typically lower than 1 % compared to the annual solar field output.

In a typical parabolic trough solar field arrangement the first row will not be shaded provided that no windbreaker or similar equipment is installed. This would reduce the value of row-to-row shading for the whole solar field by approximately 1 %. Furthermore a small fraction of the rows is not shaded by others in case that the sun azimuth angle is not exactly perpendicular to the collector azimuth angle. Both effects can be calculated solely by simple geometrics but they are really small and it is recommended to neglect them as a conservative approach, at least for large solar fields of several 100,000 m². Actually, they may reduce the annual losses caused by row-to-row shading by 2 or 3 %, considering that these losses only amount to approx. 1 % of the annual heat production of the solar field, and even less for the annual electric energy yield. These numbers are valid for large parabolic trough fields of several 100,000 m² and should be revised in case that the solar field under investigation consists only of a few single collector rows!

The next equation allows correction of the shading efficiency of a complete solar field considering unshaded rows at the boundary.

$$\eta_{\text{shad}} = \frac{n_{\text{row}}}{n_{\text{row}} - n_{\text{row, unshad}}}\ \eta_{\text{shad,row}} \tag{C.14}$$

Other shading effects

An additional shading parameter a_{shad} is included into the shading equation in order to account for shading caused by buildings or other obstacles close to the solar field.

$$\eta_{\text{shad}} = \eta_{\text{shad,row}} - a_{\text{shad}} \tag{C.15}$$

Buildings may be located within the solar field itself (e.g. cooling towers, wind breakers) or outside the solar field area but close to the boundary.

Mountains at the horizon should already be considered in the meteorological dataset in a manner that G_{bn} will be zero as long as the sun is behind the mountains. If there are mountains at the horizon, modelers shall check whether the elevated horizon line is considered in the meteorological dataset or not.
In case that the solar field area is made of terraces, additional shading caused by these terraces must be considered. Due to the manifold of different external shading reasons no general formula for the calculation can be given here. Many solar fields are built in a manner that α_{shad} is almost zero but this assumption must be checked prior conducting a performance simulation.

Soiling

Since parabolic trough plants are large outdoor installations, they cannot be considered as perfectly clean and thus the mirrors and receivers show reduced reflectivity and transmission compared to laboratory measurements. In order to minimize soiling losses, parabolic trough plants are cleaned periodically. The soiling rate and the frequency of cleaning is site-specific and is a part of the O&M concept. Generally, cleanliness varies with time and location within the solar field. Cleaning of the whole field needs typically several nights (see also Appendix L, Local Site Conditions).

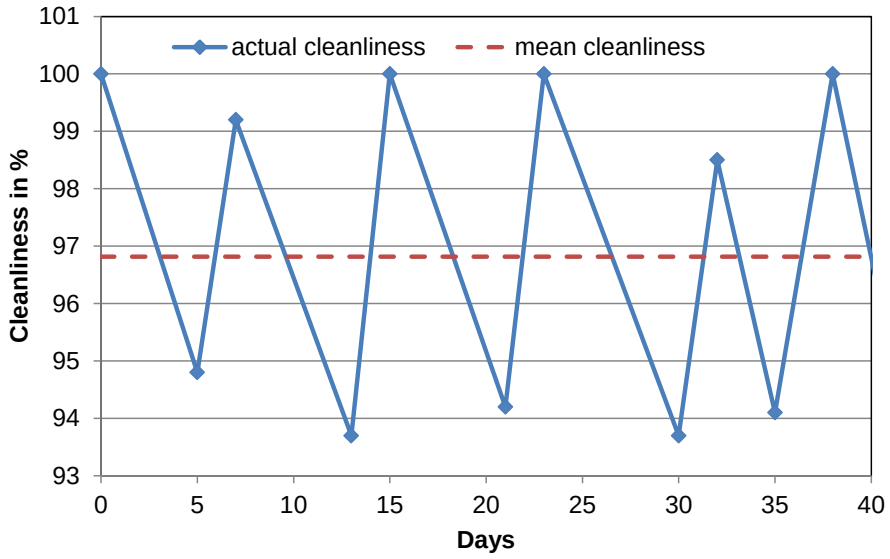

Figure C-7: Example for the course of actual and mean reflectivity of parabolic trough mirrors

A common approach to consider soiling in annual performance models for parabolic trough plants is the utilization of a mean effective cleanliness factor without any variation in time and space. This **effective mean cleanliness factor** just describes the reduction of the solar field efficiency caused by soiling with a single value valid for the whole field and over the whole time period simulated.
The cleanliness factor is defined by the ratio of optical efficiency in certain dirty conditions and the optical efficiency with the same optical element in unsoiled, clean condition. This factor can be applied to single components (mirror, receiver), or to the whole collector.

$$\eta_{\text{clean}} = \frac{\eta_{opt,0,soiled}}{\eta_{opt,0}} \quad \text{(C.16)}$$

Time and space resolved cleanliness factors could be used in principle in annual performance models but it is not recommended in general since this approach would need more information about soiling conditions and cleaning procedures at site. It should be dedicated to special simulations dealing with this effect. Instead, the intention here is to consider soiling as an important general effect for performance reduction and apply the same cleanliness factor for the whole solar field.

Peak optical efficiency

Peak optical efficiency is the ratio of power absorbed by the receiver and available solar power. It considers the reflectivity and shape deviations of the mirrors, shading and blocking by structural elements of the collector, reflection and absorption at the receiver glass cover, intercept efficiency, and imperfect absorption of the receiver. The peak optical efficiency is typically measured using a complete collector under the following boundary conditions:

- Incidence angle is perpendicular to the collector aperture
- The collector is perfectly clean
- No external shadows are on the aperture

Normally, the peak optical efficiency is provided by parabolic trough suppliers. Since the available solar power depends on the definition of the collecting area, the peak optical efficiency shows this dependency, too. Thus, it is very important to know the corresponding collecting area when using a certain value of the peak optical efficiency.

The utilization of nominal aperture area (see nomenclature) and the corresponding nominal peak optical efficiency is recommended in order to have a common base for comparison. It is typically given for a single collector unit (e.g. for Eurotrough with 150 m length and 5.77 m width) but can also be used for a whole loop or even the whole solar field, provided that identical collectors are used. This is because effects like row-to-row shading, end losses, etc., are calculated separately.

$$\eta_{\text{opt},0} = \frac{\dot{Q}_{\text{Abs},0}}{G_{\text{bn}}\ A_{\text{nom}}} \quad \text{(C.17)}$$

It should be mentioned that with this definition, for parabolic trough collectors, the peak optical efficiency includes also the optical effects of the receiver. Therefore the value of the peak optical efficiency will change when another type or size of receiver is installed.

Incidence angle modifier

Most of the time parabolic trough aperture is not perpendicular to the incoming sun rays. The non-zero incidence angle causes additional losses (supplementary to cosine losses) due to:

- The sun is actually not a single point but rather a disk with a certain size. Therefore, the radiation onto an infinitesimal element on the collectors mirror surface can be considered as a cone having a half angle of 16' (calculated from the sun's diameter and the mean distance

between sun and earth). The reflected beam also has the shape of a cone with the same angle. With increasing incidence angle the distance for the reflected sun rays between mirror and receiver increases which causes a larger image of the sun. Since the receiver tube has a certain diameter, this effect may increase the fraction of sun rays which are not hitting the receiver tube (also known as spillage).

- The same physical effect will add optical losses with angular dependencies which are caused by the above mentioned imperfect surface and shape of the mirrors.
- The collector structure has a limited stiffness. Therefore deformation of the parabola may occur depending on the collector track angle.
- Angular dependency of the reflection at the receiver glass envelope. Glass envelopes typically have an anti-reflective coating to minimize this effect; nevertheless the efficiency of this anti-reflective coating is limited.
- The receiver tubes need to be mounted onto the parabolic trough with structural elements and these elements may cause shading of the mirror surface and/or the receiver surface. The impact of these shading effects depends on the incidence angle.

The so called incidence angle modifier (IAM) is used to account for all these optical losses which depend on the incidence angle of the sun rays onto the aperture. It is defined[1] as:

$$K(\theta_\mathrm{i}) = \frac{\eta_\mathrm{opt}(\theta_\mathrm{i})}{\eta_\mathrm{opt,0}} \tag{C.18}$$

The IAM is typically measured at a single collector or determined by detailed ray tracing simulations and provided by suppliers as polynomial or lookup table as a function of the incidence angle. Often, the proposed IAM functions have the structure

$$K(\theta_\mathrm{i}) = 1 + \sum_{k=1}^{n} \frac{a_k \theta_\mathrm{i}^k}{cos(\theta_\mathrm{i})} \tag{C.19}$$

With a_k representing the polynomial coefficients and *n* representing the order. Other mathematical forms of the IAM polynomial are published and this guideline will not recommend a particular one. Sometimes, the cosine losses are already included in the IAM function provided by suppliers or from literature; this has to be checked by the user prior to the application of a new equation.
The recommendation of this guideline is to calculate both effects separately for parabolic trough collectors.

[1] This definition needs tob e cross-checked with the definition of eta_opt and the definition of the incident angle modifier in Appendix T

$$K' = cos(\theta_i) \cdot K \quad \text{(C.20)}$$

Due the variety of IAM equations, users have to check the correct utilization when using published data from other sources. One simple check is to plot the given IAM function in comparison to the cosine losses, like in Figure C-8. For parabolic trough collectors, the IAM' curve is below the cos(θ_i) curve whereas the IAM curve is typically above at least for most incidence angles. If this not the case, users should check the definition of their IAM equation carefully.

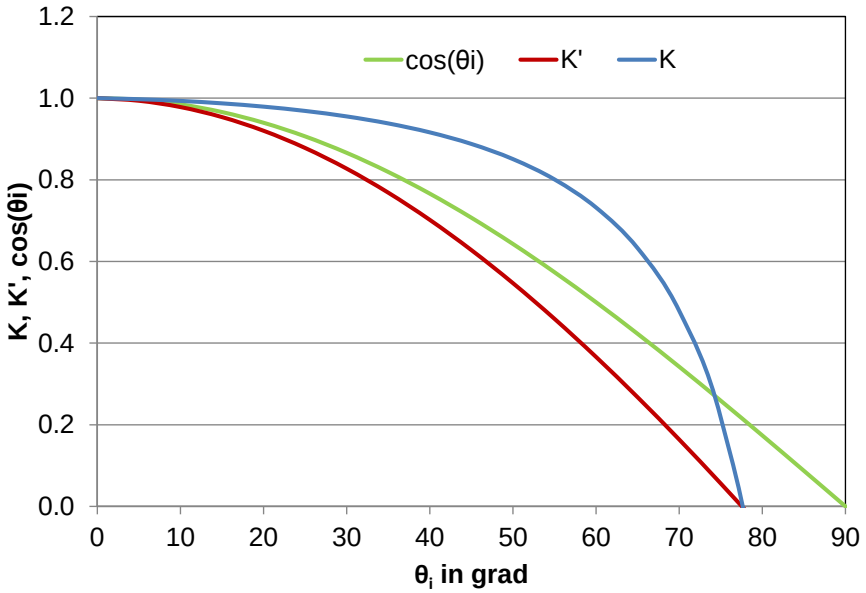

Figure C-8: Plot of a typical K, cos(θ_i) and K' functions for a parabolic trough collector

End losses are also not included in the IAM function but shall be modelled separately.

End losses

The following figure shows a sketch of two collectors in a row with the focal length f (vertical distance between receiver axis and mirror surface) the collector length l_{col} and the axial distance between the collectors d_{col}. In the shown case, sun beams are not perpendicular to the aperture of the collector. The sun beam impinging upon a collector's edge is reflected but does not hit the receiver of this collector. Hence, regarding the left collector, a part of the receiver with the length $l_{endloss}$ is not irradiated and does not contribute to the heat production.

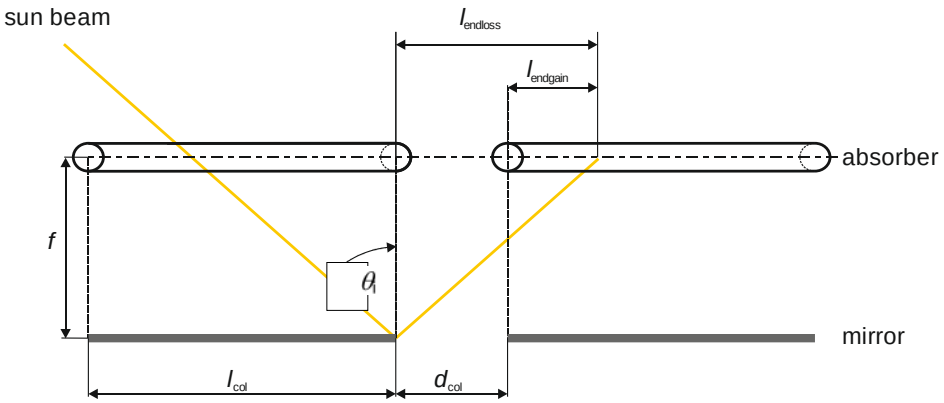

Figure C-9: End losses and end gains for parabolic trough collectors (taken from guiSmo)

The endloss efficiency is be determined by

$$\eta_{\text{endloss}} = 1 - \frac{l_{f,aver}\, tan(\theta_i)}{l_{col}} \tag{C.21}$$

Eq. (C.21) is valid for a single collector and also for the whole loop, provided that it is made of identical collectors.
It should be mentioned that the average distance between reflector and receiver is not equal to the focal length for parabolic trough collectors. For parabolic trough collectors using a single parabola like the Eurotrough collector, the average distance between reflector and receiver can be calculated from:

$$l_{f,aver} = f\left(1 + \frac{w_{col}^2}{48 f^2}\right) \tag{C.22}$$

For the Eurotrough collector e.g. the focal length is 1.71m but the average distance between reflector and receiver is 2.11m! This formula is not valid for collectors like the Ultimate Trough since the outer mirrors of this collector type are staggered. They have different focal lengths and the average distance cannot be calculated by the simple formula given above (f_1=1.71m, f_2=1.88m, $l_{f,aver}$ = 2.51m, [Riffelmann 2011] and [Riffelmann 2014]).

In the case of several collectors in a row the end losses can be partially compensated. As shown in Figure C-9 the representative sun beam hits the receiver of the neighboring collector. End losses and the degree of compensation by end gains depend on focal length, collector length and distance between collectors in a row. In real solar field installations end gains hardly occur since they require perfect alignment and perfect adjusted tracking of adjacent collectors, which does often not exist. Therefore, it is recommended to neglect this potential effect for annual performance models. The impact of neglecting end gains is low and it is a conservative approach to calculate the annual plant output.

The equation for calculating end losses with consideration of end gains for a row is:

$$\eta_{\text{endloss}} = 1 - \frac{l_{\text{f,aver}}\, tan(\theta_i)}{l_{\text{col}}} + max\left[\frac{\left(n_{\text{col,row}} - 1\right)}{n_{col,row}} \cdot \frac{l_{f,aver}\ \tan(\theta_i) - d_{col}}{l_{col}}\ , 0\right] \qquad \text{(C.23)}$$

For the typical solar field all rows are identical, thus the equation is also valid for one loop and for the whole solar field. Eq. (C.23) considers that for the last collector in a row there will be no end gains.

Solar field availability

The solar field is designed and built with a certain number of troughs, mirrors and receivers but experience from existing plants shows that a certain fraction of the solar field is often not available because of different reasons. Reasons for reduced availability of the solar field are among others: broken mirrors, collectors with damaged drives, loops which need maintenance etc.
All these effects reduce the actual aperture which can be used to collect heat. In order to account for these effects, an availability factor for the solar field is defined with values between 0 and 1. For typical commercial CSP plants with suitable maintenance of the solar field, the solar field availability is usually close to 1; i.e. almost 100 % of the aperture is available

$$\eta_{avail}^{\text{SF}} = \frac{A_{\text{nom,reduced}}}{A_{\text{nom}}} \qquad \text{(C.24)}$$

The solar field availability does not cover losses caused by system outages. It is only a reduction of usable solar field aperture. In addition to that, CSP plants (like other technical installations) will show forced outages as well as planned outages. They will reduce the output of electricity. In principle, they may be divided into three groups:

- The whole plant is not available due to defects, failures and damages of main systems (main HTF pumps, cooling system etc.)
- The whole plant is not available due to a scheduled maintenance period
- The CSP plant would be able to produce but the grid cannot accept power due to any reason.

This guideline recommends considering these outages rather in the financial model (see Appendix N) and not in the solar field performance model. The reason is to combine outages for the whole plant and consider them all together at a suitable point of the model. See also chapter 9.2 of the Guideline.

Wind impact

In the specifications of parabolic trough collectors, three important wind velocities are given: the design wind speed, the maximal operation wind speed, and the survival wind speed. The first two values are important for performance modelling because up to the design wind speed nominal

efficiency should be reached. Above this design wind speed, presumably the efficiency of collectors will be reduced by induced oscillations and deformation of the reflecting surfaces, or tracking errors. Systematic research and models for this effect are hardly available today. Even if the wind impact on the optical performance is known for a single collector, it may change significantly in a large solar field with many other collectors, or when a wind breaker fence at the solar field boundaries is installed, etc. In order to consider this effect in annual performance models, more data from suppliers or independent laboratories must be available.

On the other hand, each collector has a certain maximal operation wind velocity above which it must be turned into stow position in order to avoid damages. It is obvious that in these cases there will be no heat production and this effect should be considered in annual performance models. The survival wind speed has no impact on the performance but rather on the plant design.

In order to estimate the impact of time periods with wind velocities between nominal and shut off wind speed, one example dataset has been analyzed in detail. Figure C-10 shows a plot of wind velocities over DNI for the 10 minutes TMY datasets for the PSA (Spain). From this plot, it is obvious that there is no correlation between wind speed and DNI. This conclusion is also valid for many other sites. On the other hand, summing up all DNI values for time periods with wind velocities above 7 m/s and below 14 m/s (that means between design wind speed and shut off wind speed) results in 308 kWh/m² which is about 14 % of the total DNI resource (2162 kWh/m²). This fraction shows that the wind impact on annual yield might actually be significant.

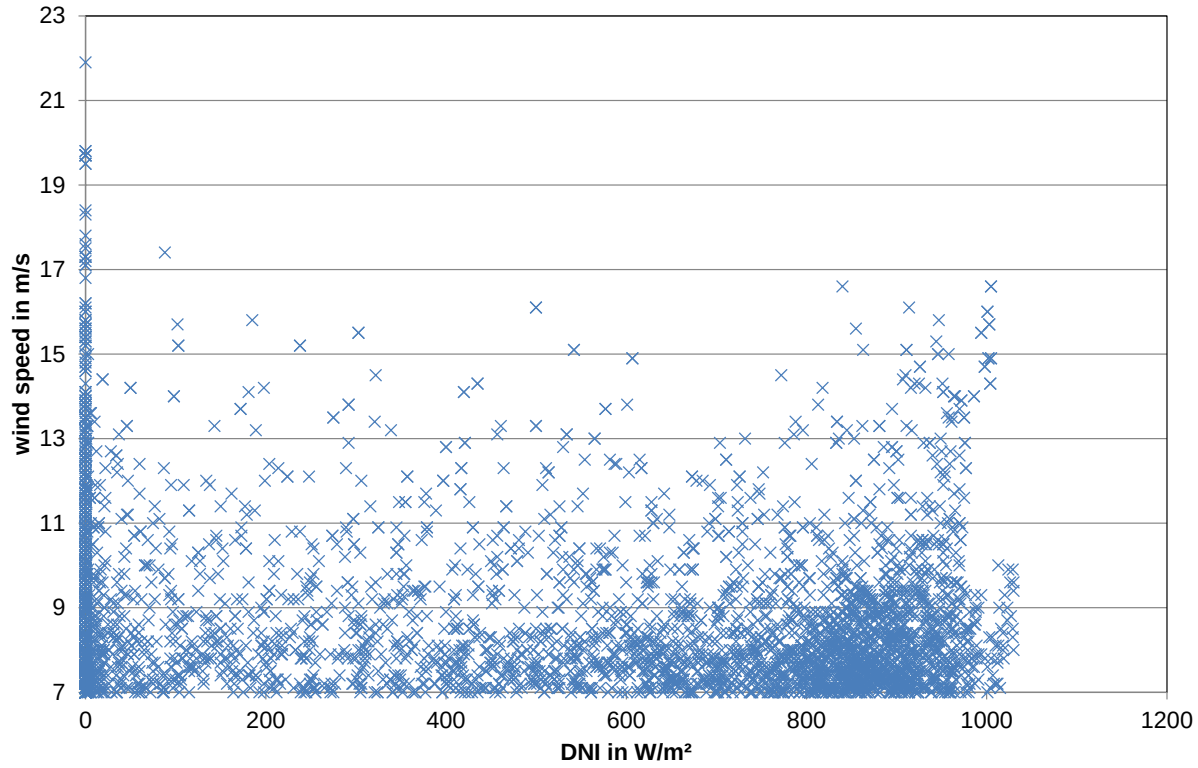

Figure C-10: Plot showing wind velocities over DNI for the TMY at PSA (Spain), 10 minutes mean values.

For the example dataset of the PSA two different scenarios have been investigated and annual yield was compared to the base case which does neglect any wind impact on the annual yield. These scenarios are:

1. The relative optical efficiency is reduced from 1.0 at 7 m/s down to zero at 14 m/s
2. The relative optical efficiency is reduced from 1.0 at 7 m/s down to 0.5 at 14 m/s

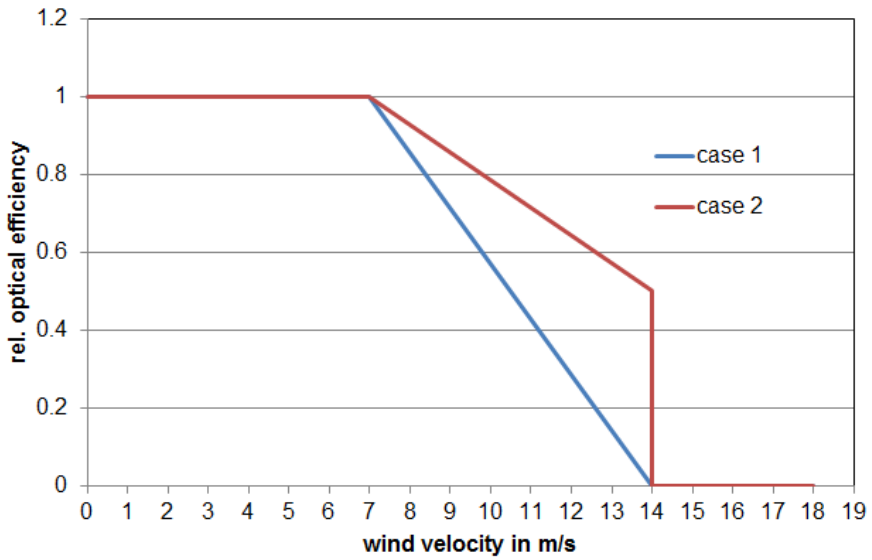

Figure C-11: Assumed dependency of relative optical efficiency and wind velocity

There was no dependency on wind directions in this assumption but all wind directions were considered as having the same effect. The application of these two scenarios for annual yield calculations results in a reduction of annual electrical yield of 2.5 % and 1.1 % respectively. Although case 1 might be considered as too pessimistic, case 2 shows that more research needs to be done about wind impact.
Meanwhile, an approach like the one shown above with a relative optical efficiency depending on wind velocity for each time step is recommended. Alternatively, a lump-sum reduction of the annual electrical output may be considered. The actual reduction depends of course on the wind conditions at site and also on the solar field design (e.g. the existence of a wind breaker fence).

Other effects

This chapter summarizes effects which obviously will have an impact on the performance but currently the impact cannot be calculated in detail because systematic measurements and applicable models are not available. As long as this situation prevails, they are considered implicitly in the uncertainty. Once models are available, these effects should be included in the general performance equation and the uncertainty might be reduced.

Sun shape

Direct normal irradiance today is measured by instruments with a certain acceptance angle which is about 10 times larger than the solar disk angle [Wilbert 2014]. Therefore, G_{bn} measurements contain a certain fraction of scattered radiation, which is called circumsolar radiation. This circumsolar radiation can only partially be used by concentrating collectors. Furthermore, it varies for different sites and is time dependent. The normalized radiance profile as function of the angular distance from the center of the sun is denoted as "sun shape" and [Wilbert 2014] has shown that the impact of the sun shape on annual yield of a trough plant might be an overestimation up to 0.5 to 1.1 % depending on the site. The lower value has been calculated for a Spanish site with lower circumsolar radiation and the upper value for Abu Dhabi with high circumsolar radiation. It should be mentioned that the reference was a disk sun shape with almost no circumsolar radiation.

The annual yield calculations of [Wilbert 2014] are based on ray tracing simulations while the optical efficiency of parabolic trough collectors is typically determined under outdoor conditions. Thus, the measured optical efficiency of parabolic troughs already includes the sun shape effect at least for the conditions available during the measurement. This would reduce the overestimation mentioned above. Nevertheless, the sun shape during efficiency measurements for parabolic troughs is typically not reported in supplier's datasheets and Wilbert's results show that further investigation will be necessary; particularly for solar tower systems where the impact of sun shape is even higher. For some collectors, the optical efficiency is not measured but rather determined by ray tracing simulations. In this case, the annual performance simulation might even show an underestimation of up to 0.4 % when the actual sun shape at site has less circumsolar radiation than the sun shape used in the ray tracing model.

Dew impact

At many sites, the mirrors may be covered by dew in the morning which prevents reflection and thus heat production. Although this effect has been observed at several parabolic trough plants, there is currently no model available. Most of the existing meteorological stations at CSP sites do not monitor dew and it is not possible to calculate the occurrence simply from ambient temperature and humidity. Radiation between the mirror surface, sky and the environment is also important. Therefore, dew impact is currently neglected in annual performance models. Beside the "blindness" of mirrors, dew might have two more effects on solar fields: increased corrosion and increased adhesion of dust on the wet mirrors. Again models for these effects are currently not available.

Snow impact

Snow will not be an issue for many CSP sites but it may occur at some of them. Similar to dew, snow will also prevent reflection. The typical meteorological datasets do not mention snow, therefore it cannot be considered in the models. On the other hand it has been reported by plant operators, that snow provides a very effective cleaning of the mirrors.

Table C-6 gives an overview about these effects which are currently not considered in the model as well as estimated about their impact on annual output. As long as no model details are available for them, the recommendation is to consider these effects in the uncertainty analysis (see chapter 9.3 of the Guideline).

Table C-6: Effects not considered in the annual performance model

Neglected effect	Effective direction	Estimated impact on annual performance
Sun shape	↗ , ↘	+0.4….-1.1 %
Dew impact	↘	0….-0.5 %
Snow impact	↘	0….-0.5 %

C.2.1.3. Thermal losses

Thermal losses for a parabolic trough solar field can be divided into several individual effects and allocated to certain parts of the solar field.

$$\sum \dot{Q}_{\text{loss}} = \dot{Q}_{\text{loss,rec}} + \dot{Q}_{\text{loss,pipe}} + \dot{Q}_{\text{loss,head}} + \dot{Q}_{\text{loss,equ}} \quad \text{(C.25)}$$

With:

$\dot{Q}_{\text{loss,rec}}$	receiver heat losses in W
$\dot{Q}_{\text{loss,pipe}}$	heat losses of the loop piping in W
$\dot{Q}_{\text{loss,head}}$	header and runner heat losses in W
$\dot{Q}_{\text{loss,equ}}$	heat losses of other SF equipment (like tanks, vessels, etc.) in W

Receiver thermal losses

Parabolic trough collector fields are equipped with thousands of meters of receiver pipes to collect the concentrated irradiation and to enable heat transfer to the fluid as well as transportation of the fluid. These pipes experience thermal losses caused by the following three mechanisms: conduction, convection, and radiation. The receiver pipes are designed and manufactured in order to minimize thermal losses. They typically:

- have a selective coating to minimize radiative heat losses,
- are equipped with a glass envelope enclosing the absorber pipe in vacuum to minimize convective losses,
- have small and insulated supports to minimize conductive losses.

Despite these measures the receiver heat losses are not negligible and induce a significant reduction of the net heat generation of parabolic trough solar fields. For state-of-the-art parabolic trough receivers, heat losses at nominal operating conditions are in the range of 10 % of the total heat absorbed.

Unfortunately, standards about testing this kind of receivers and reporting test results are not available today. Therefore, several approaches exist in parallel and often they cannot be transformed easily into each other. Thermal receiver losses are often given as polynomial or lookup table and are provided by suppliers or published by laboratories. In the following chapter, several approaches are shown and discussed. Often, annual performance models must use what they get as input for receiver heat losses and the options for manipulation of the given equations are limited. The paragraphs show some pitfalls which must be obeyed when using or extending receiver heat loss equations from literature.

[Dudley 1984] proposed a second order polynomial with an additional linear term containing G_{bn} in order to account for the fact that higher irradiance should have an impact on absorber surface temperatures. His model equations for specific receiver heat losses (in W/m of receiver length) are based on the bulk HTF temperature.

$$\dot{q}_{\mathrm{loss,rec}} = IAM'\, G_{\mathrm{bn}} a_0 (\vartheta_{HTF} - \vartheta_{amb}) + a_1 (\vartheta_{HTF} - \vartheta_{amb}) + a_2 (\vartheta_{HTF} - \vartheta_{amb})^2 \qquad \text{(C.26)}$$

Most of the empirical heat loss equations cited in this chapter are written with temperatures in °C. In this handbook we recommend to use rather K but as long as temperature differences are used, both approaches are equivalent.
[Burkholder 2009] cites the equation from [Price 2003] which is also used in the SAM empirical model.

$$\begin{aligned} \dot{q}_{\mathrm{loss,rec}} = {} & b_0 + b_1 (\vartheta_{HTF} - \vartheta_{amb}) + b_2 \vartheta_{HTF}^2 + b_3 \vartheta_{HTF}^3 \\ & + b_4 G_{\mathrm{bn}} IAM\, cos(\theta_i)\, \vartheta_{HTF}^2 \\ & + \sqrt{v_{wind}} \left(b_5 + b_6 (\vartheta_{HTF} - \vartheta_{amb}) \right) \end{aligned} \qquad \text{(C.27)}$$

This equation considers the impact of HTF temperature (represented by b_2 and b_3), the impact of absorber temperature (b_4), ambient temperature, and wind (represented by b_1, b_5 and b_6). For evacuated receivers with intact glass covers, the impact of ambient conditions is small and the HTF temperature is the dominating parameter (Figure C-12 and Figure C-13). From Figure C-12 it is obvious that the function has a lower limit temperature below which the validity is questionable. The plotted curves show an intersection at about 150 °C which cannot be explained by physically means.
[Burkholder 2009] calculated the coefficients of equation (C.27) using a model developed by [Forristall 2003] and fitting the parameters of this equation to heat loss measurements. The Forristall model needs additional input parameters like absorptance and emittance of the absorber and transmittance of the glass envelope. These values are not generally available, therefore a simpler approach must often be chosen.

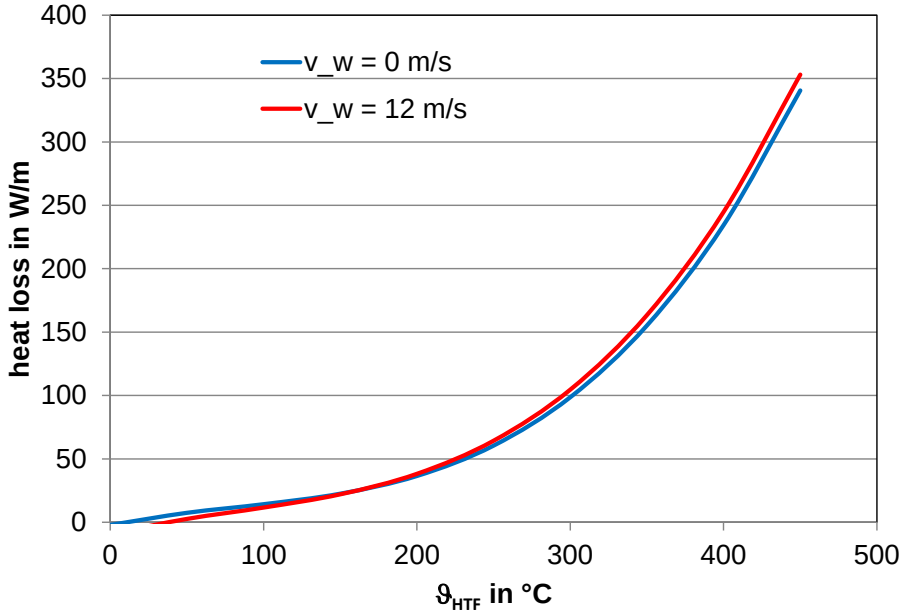

Figure C-12: Impact of wind velocity on receiver heat losses for a Schott PTR 70 receiver according to eq. (C.27) (Coefficients from [Burkholder 2009])

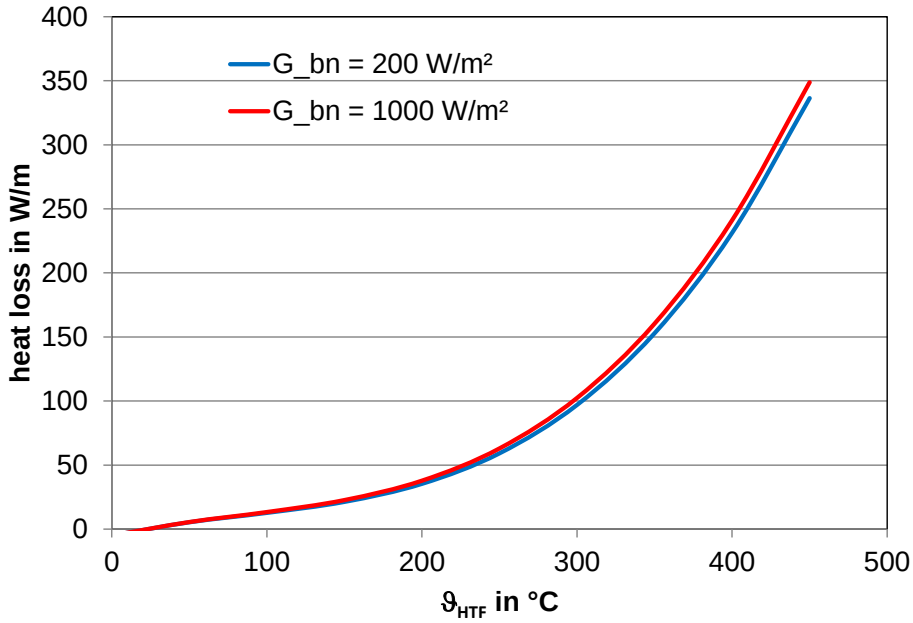

Figure C-13: Impact of beam irradiance on receiver heat losses for a Schott PTR 70 receiver according to eq. (C.27) (Coefficients from [Burkholder 2009])

Currently, thermal receiver tests are typically performed in laboratories by heating a single receiver electrically from inside to a certain temperature and measure the heat losses for this stagnant temperature. The test results are reported typically as an approximating equation for the measured specific heat losses per meter of receiver tube with the receiver temperature as independent

parameter. This function is often a polynomial up to fourth order since radiation is the dominating heat loss effect and a fourth order equation provides often good approximation for the measurements.

$$\dot{q}_{\mathrm{loss,rec}} = a_0 + a_1(\vartheta_{abs} - \vartheta_{amb}) + a_2(\vartheta_{abs} - \vartheta_{amb})^2 + a_3(\vartheta_{abs} - \vartheta_{amb})^3 + a_4(\vartheta_{abs} - \vartheta_{amb})^4 \quad \text{(C.28)}$$

Today, laboratory tests are often just using the following equation for specific heat losses [Burkholder 2009], [Pernpeintner 2012]:

$$\dot{q}_{\mathrm{loss,rec}} = a_1\vartheta_{\mathrm{abs}} + a_2\vartheta_{abs}^4 \quad \text{(C.29)}$$

This equation has two problems considering the direct utilization in annual performance models: the utilization of the absorber temperature rather than the bulk fluid temperature and the missing dependency on ambient temperature. One argument for the latter simplification is that all measurements are done at the same ambient temperature and that this ambient temperature is quite low compared to the absorber temperature (at nominal conditions).
Laboratory measurements of receiver heat losses like those reported in [Burkholder 2009] are made with an electrical heating element inside the absorber tubes. The absorber temperature at the inner side is measured together with the electrical power needed to keep the whole tube at this temperature at steady state conditions. In an operating parabolic trough plant the absorber surface temperature will not be the same as the bulk HTF temperature. A certain part of the absorber circumference will be hit by concentrated sunlight and may have a higher temperature than the bulk HTF. The remaining part of the absorber circumference might show lower temperatures. Annual performance models will rather use the bulk HTF temperature of the fluid instead of the absorber surface temperature in order to simplify the calculation. [Burkholder 2009] has calculated a temperature difference of 1 to 4 K between the inner side of the absorber tube and the bulk fluid temperature dependent on the beam irradiance. The higher value of 4 K has been calculated for G_{bn}=800 W/m² and using the laboratory heat loss curve assuming that bulk fluid temperature and inner absorber temperature are identical would result in an underestimation of heat losses of 3.4 % at 350 °C mean fluid temperature for the DPO/BP system.
[Duffie 1991] and [Lüpfert 2004] propose to use a heat loss efficiency factor *F'* to account for the temperature difference between bulk HTF and wall temperature and write the heat loss equation with the temperature difference between bulk fluid and ambient. The physical interpretation of this efficiency factor is the ratio of the total heat transfer coefficient from fluid to ambient to the heat transfer coefficient from absorber tube to ambient. With this factor equation (C.28) becomes:

$$\dot{q}_{\mathrm{loss,rec}} = F' \cdot [a_0 + a_1(\vartheta_{HTF} - \vartheta_{amb}) + a_2(\vartheta_{HTF} - \vartheta_{amb})^2 + a_3(\vartheta_{HTF} - \vartheta_{amb})^3 + a_4(\vartheta_{HTF} - \vartheta_{amb})^4] \quad \text{(C.30)}$$

For typical parabolic trough systems with HTF inlet temperatures at about 290 °C and outlet temperatures at about 390 °C the utilization of bulk fluid temperature instead of absorber surface temperature in equations (C.28) and (C.29) will cause an underestimation of 1 to 3 % of the heat losses. Considering that the receiver heat losses are about 10 % of the total heat absorbed, the resulting error might be neglected for these systems.
Sometimes heat loss or efficiency measurements are available for a whole collector or a whole loop. In contrast to the laboratory measurements for single absorbers they have been done under real operating conditions and the bulk fluid temperature is measured and reported. In these cases, no correction factors would be necessary and the functions can be used directly to model heat losses. In any case, the description for an individual performance model shall contain information about the heat loss function together with reference to the origin, the range of validity, and modifications made in order to use it for annual performance simulation.

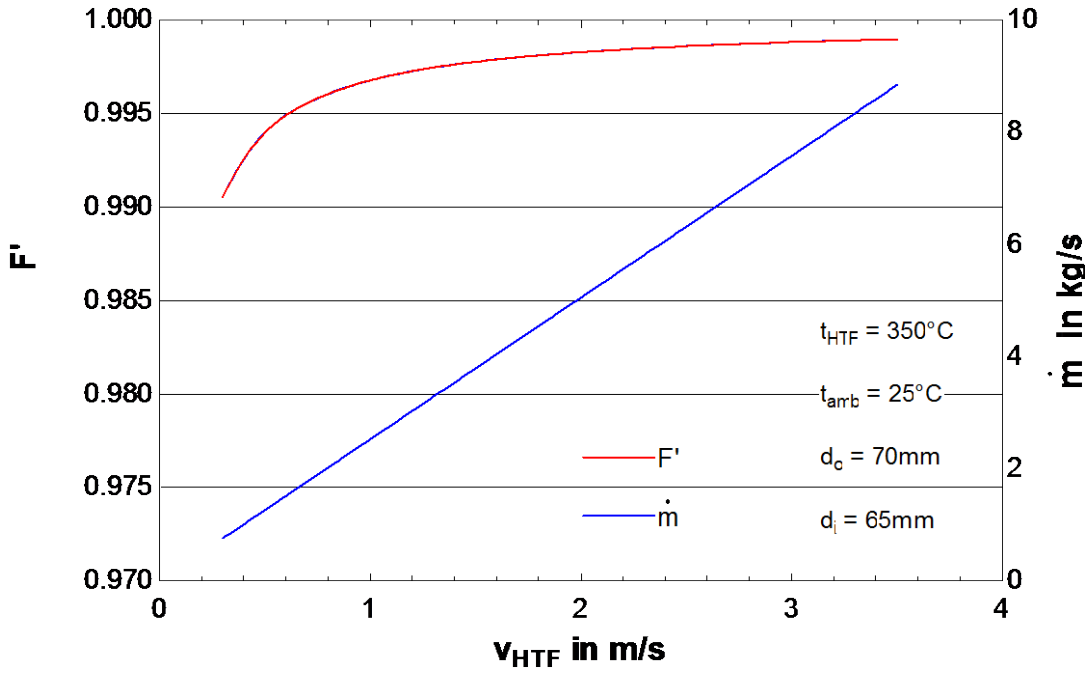

Figure C-14: Factor F’ and HTF mass flow rate for a receiver tube with VP-1 at typical operation conditions over HTF velocity

The problem that Eq. (C.29) does not consider ambient temperature, can be resolved by using an own approximation of the measurements with the temperature difference between absorber and ambient. The test reports typically contain the ambient temperature during the measurements and thus it is an easy task to make a new approximation. This is of course only a first approach but it is necessary in order to use the heat loss equations for the simulation of heat up and cool down of the solar field. Nevertheless, the utilization of approximations for extrapolation might cause severe errors if they are not checked carefully. The following example will show this in detail. It is based on published measurements of a Schott PTR 70 receiver pipe [Pernpeintner 2012]. The blue squares in Figure C-15 to Figure C-17 are the measured data points. The lowest temperatures of these measurements are at

227 °C above ambient. The annual performance model will need to calculate heat losses at significant lower temperature differences for night time cooling down simulation. Thus approximations were made in order to get an equation which might be used for the whole temperature range from ambient temperature up to maximum absorber temperature. From Figure C-15 it is obvious that a second order polynomial is not suitable whereas Figure C-16 shows that the 4th order polynomial, which goes through the origin, might be a reasonable approximation in this case. Further constraints might be used to get a physically meaningful approximation: first and second derivatives should be always larger than zero in the relevant temperature range.

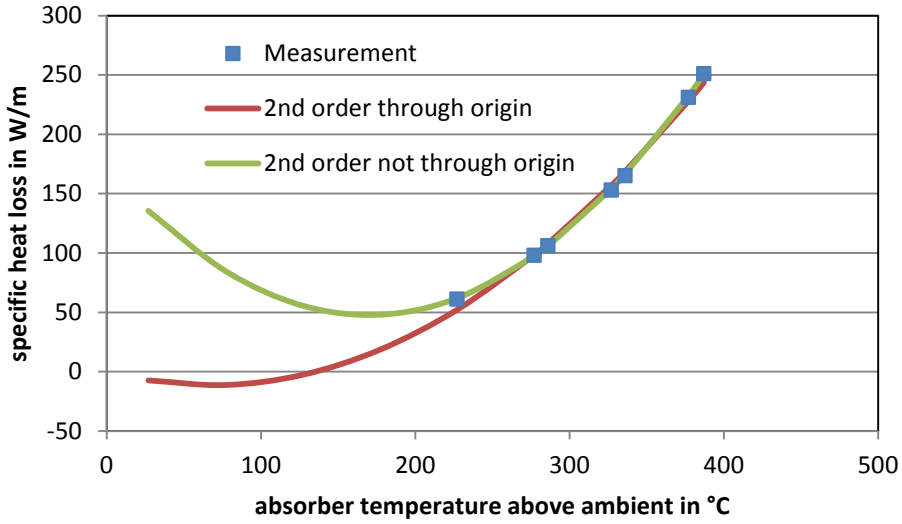

Figure C-15: Approximation of receiver heat losses by 2nd order polynomials

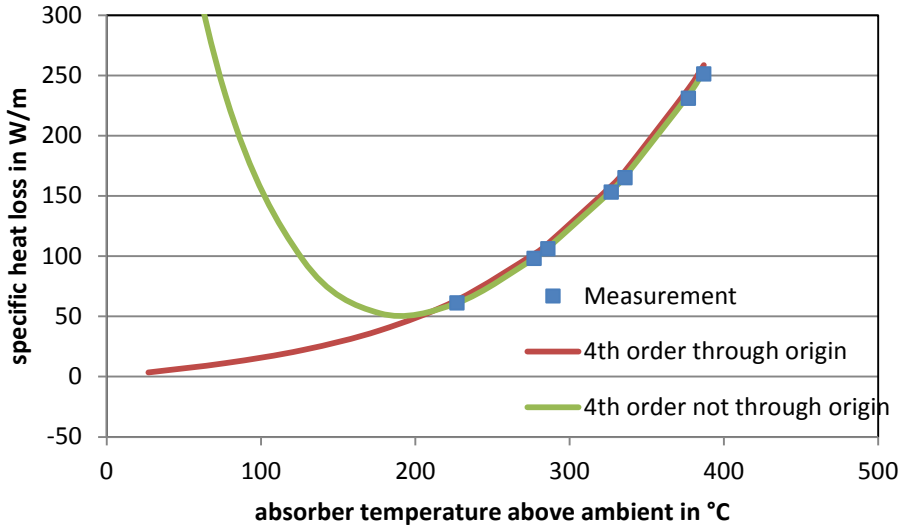

Figure C-16: Approximation of receiver heat losses by 4th order polynomials

Figure C-17 shows that a spline approximation will be even better in the sense that it will meet the measurements. This example shows that the user must be very cautious when using approximations for extrapolation and check that the approximation will give physically reasonable results for the whole temperature range. In general, it would be desirable to get more measurements also for low absorber temperatures from the modeler's point of view.

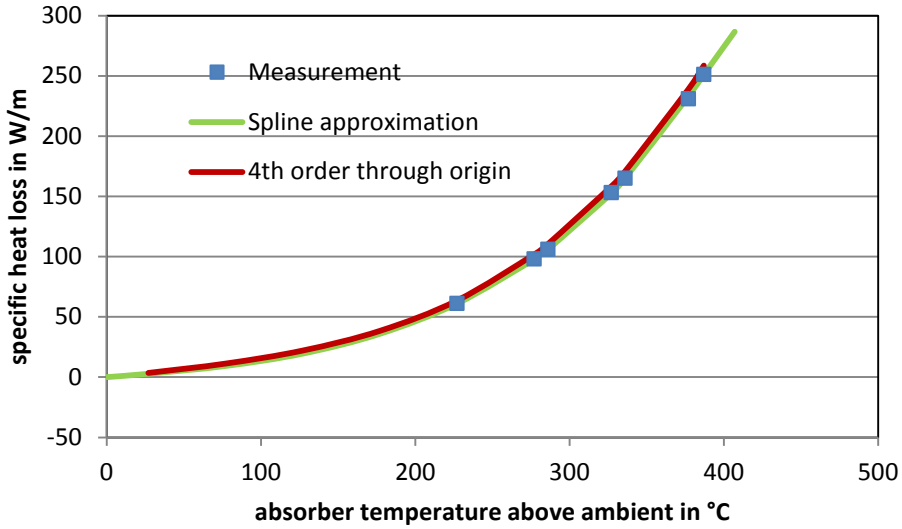

Figure C-17: Approximation of receiver heat losses by splines

Another important question is whether one single mean temperature between solar field inlet and outlet would be sufficient to model the heat losses or whether more nodes are necessary. [Wittmann 2012] published a paper on this topic, concluding that the underestimation of heat losses for typical parabolic trough systems with thermal oil and 290 °C/390 °C temperatures is in the range of 3-5 % when using just one single mean temperature. Again, this might be negligible for annual performance simulations since the impact on annual thermal output will be an over estimation in the range of 0.5 %.

For parabolic trough systems with considerable higher outlet temperature and temperature rise, [Wittmann 2012] proposes the utilization of a correction factor when using a single temperature node over the whole loop for heat loss calculation.

$$\dot{q}_{\mathrm{loss,corr}} = f_{\mathrm{corr}} \cdot \dot{q}_{\mathrm{loss,rec}} \qquad \text{(C.31)}$$

The correction factor f_{corr} may be calculated for the specific system in a separate model with high spatial resolution for the whole loop. Main parameters for the correction factor are beam irradiance and inlet and outlet temperature of the loop, thus the correction factor will depend on solar field load.

Thermal losses of field piping and header system

In parabolic trough solar fields, the individual troughs must be connected to each other by pipes and flexible connectors. These connectors may be flexible hoses or so called ball joints and they allow for individual tracking of each single collector as well as for longitudinal expansion of the receiver pipes. Crossover pipes connect two collector rows to form a U-type loop and loops are connected by interconnecting pipes to the headers, which in turn are connected with runners. Furthermore, each loop has a number of valves for isolation, draining or venting as well as flow distribution. “Runner” pipes connect the headers with heat exchangers, which are located near the turbine. All this equipment is called "field piping" and although they are well insulated, heat losses cannot be avoided. Thermal losses for field piping and headers can be calculated by detailed models from pipe diameters, HTF masses and temperatures, type and thickness of heat insulation, etc. but often it is sufficient to consider overall heat losses in terms of watt per square meter of aperture and mean temperature difference between solar field and ambient. Another option is to define specific piping losses per length unit as for the receiver heat losses. This approach is shown in (C.32) which gives an expression for the heat losses of a single loop.

$$\dot{Q}_{loss,loop} = n_{coll,loop}\, n_{rec,coll}\, l_{\mathrm{rec}}\, \dot{q}_{\mathrm{loss,rec}} + l_{pipe,loop}\, \dot{q}_{\mathrm{loss,pipe}} \qquad \text{(C.32)}$$

The typical piping length for one loop made of four Eurotrough 150 collectors is about 60-70m (including swivel joints, cross over pipe, connecting pipes to headers and valves but excluding the receivers). Piping heat losses depend of course on insulation material and thickness but a first approximation for these loop piping heat losses gives 150 to 200 W/m specific heat loss, assuming an insulation layer of 40 mm thickness for a 73 mm OD (2½’’) tube and heat conductivity of 0.07 W/(m K). These values are valid for ideal conditions of insulated pipes.
The steady state net thermal power of one loop may be calculated from:

$$\dot{Q}_{\mathrm{loop,steady}} = cos(\theta_i)\; IAM\, \eta_{\mathrm{opt,0}}\, \eta_{\mathrm{shad}}\, \eta_{\mathrm{clean}}\, f_{\mathrm{focA}}\; A_{\mathrm{nom,loop}}\; G_{\mathrm{bn}} - n_{\mathrm{coll,\,loop}}\, n_{\mathrm{rec,\,Coll}}\, l_{\mathrm{rec}}\, \dot{q}_{\mathrm{loss,rec}} - l_{\mathrm{pipe,loop}}\, \dot{q}_{\mathrm{loss,pipe}} \qquad \text{(C.33)}$$

Headers and runners might be considered in one single expression; therefore the header losses shall comprise both heat losses in headers as well as in runners. Header losses can be defined as specific heat losses per meter of header length and in this case they are in the same range as the piping losses given above, thus 150 to 200 W/m. Again these values are valid for ideal conditions of insulated pipes. The larger diameters of these header pipes require thicker insulation layers which results in similar specific heat losses than for the loop piping. Similarly higher fluid temperatures inside hot headers compared to cold headers may be compensated by thicker or better insulation layers. These values for piping and header heat losses are only given for information. During the detailed engineering phase a techno economic optimization will be done in order to determine the insulation thickness. For some CSP projects, maximum acceptable piping heat losses are defined in the technical specifications of

tender documents. In this case, the value may be used as model input and the EPC contractor has to design the insulation in a manner that they are not exceeded.

Another option is to define piping and header losses based on the aperture area. In this case, corresponding specific values are 3 to 4 W/m² for loop piping losses and additional 2 to 4 W/m² for header losses (provided that collector technology and solar field layout are similar to the parabolic trough with thermal oil reference plant). These values are valid for ideal conditions of insulated pipes. In a real plant the heat losses are higher because of the need for pipe support structures were additional heat losses caused by thermal conduction occur. Furthermore, the insulation might have defects or gaps, etc. Due to these non-ideal conditions the theoretical heat losses given above shall be multiplied by a factor of 1.5 to 2 in order to adapt them to real conditions according to a typical engineering guess. Thus we have 6 to 8 W/m² for loop piping losses and another 4 to 8 W/m² for header losses for nominal conditions.

$$\dot{Q}_{\mathrm{loss,head}} = A^{\mathrm{SF}}\, \dot{q}_{\mathrm{loss,head,A}} = l_{\mathrm{head}}\, \dot{q}_{\mathrm{loss,head}} \qquad \text{(C.34)}$$

In principle, it must be mentioned which aperture definition is used for the calculation of these specific heat losses: net aperture, nominal aperture or gross aperture. Actually the values of these 3 aperture definitions will not be too different from each other but will rather be within a range of about 5 %. Since the utilization of aperture specific heat losses is an approximation and a simplification, the impact of aperture definition might be neglected and the values mentioned above may be used for each of the aperture definitions. The safety margin used above for aperture specific header and piping losses will cover these small differences in aperture area definitions.
The idea behind the utilization of aperture specific heat losses (based on solar field aperture area) is that they allow for easy variation of the solar field size and scaling header and runner heat losses just by multiplying the specific heat losses and the actual solar field aperture instead of calculating the actual header length for each configuration. Such specific header losses based on aperture area are only valid within a certain range of aperture areas and it is not correct to use the same values for very small and very large solar fields. In these extreme cases the dependency of header length and diameter on solar field size and shape must be considered when using aperture specific heat losses.
These values given above for specific piping and header losses are valid for nominal conditions. In order to use them also for heating up and cooling down during time periods without irradiance, they can be scaled linearly with the temperature difference between mean nominal solar field temperature and ambient temperature.

$$\dot{Q}_{loss,pipe} = l_{\mathrm{pipe}}\, \dot{q}_{\mathrm{loss,pipe}} = l_{\mathrm{pipe}}\, \dot{q}_{\mathrm{loss,pipe,nom}}\, \frac{(T_{HTF} - T_{amb})}{(T_{HTF,nom} - T_{amb,nom})} \qquad \text{(C.35)}$$

It is obvious that header losses will cause a certain temperature decrease. The highest HTF temperature occurs at the loop outlet and due to the header losses the inlet temperature to the HTF-

steam heat exchangers is a few Kelvin lower than the average loop outlet temperature. The HTF temperature at the heat exchangers may be calculated with the specific heat capacity c of the fluid from

$$\dot{Q}_{\text{loss,hot head}} = \dot{m}_{\text{HTF}}\, c_{\text{HTF}}\left(T_{\text{loop,out}} - T_{\text{out}}^{\text{SF}}\right) \tag{C.36}$$

This equation shows that the temperature difference depends on the HTF mass flow rate and thus on the solar field load. Assuming a constant header heat loss, the temperature at the solar field outlet (which is identical to the temperature at heat exchanger inlet) decreases with decreasing mass flow. Similarly, the loop inlet temperature is typically lower than the HTF temperature at the solar field inlet (heat exchanger outlet).

$$\dot{Q}_{\text{loss,cold head}} = \dot{m}_{\text{HTF}}\, c_{\text{HTF}}\left(T_{\text{in}}^{\text{SF}} - T_{\text{loop,in}}\right) \tag{C.37}$$

Having the temperature drop in the cold and hot header in mind, the question arises, if the mean temperature calculated from solar field inlet and outlet temperature is representative for the receiver heat losses. Despite this temperature decrease, heat losses of the representative loop of the solar field (with single phase HTF and temperatures of about 290/390 °C) can be calculated with the mean solar field temperature which was calculated using the temperatures at the interface between solar field and heat exchangers. The justification for this approach is that the temperature decrease in both headers is almost the same and thus the arithmetic mean temperature between inlet and outlet is also the same, either using the temperatures at loop inlet or at the heat exchangers (Figure C-18). The impact of this simplification on the mean solar field temperature is only in the range of 0.5 to 1 K. The higher temperature difference between hot header and ambient is typically compensated by better or thicker insulation of this header compared to the cold header.

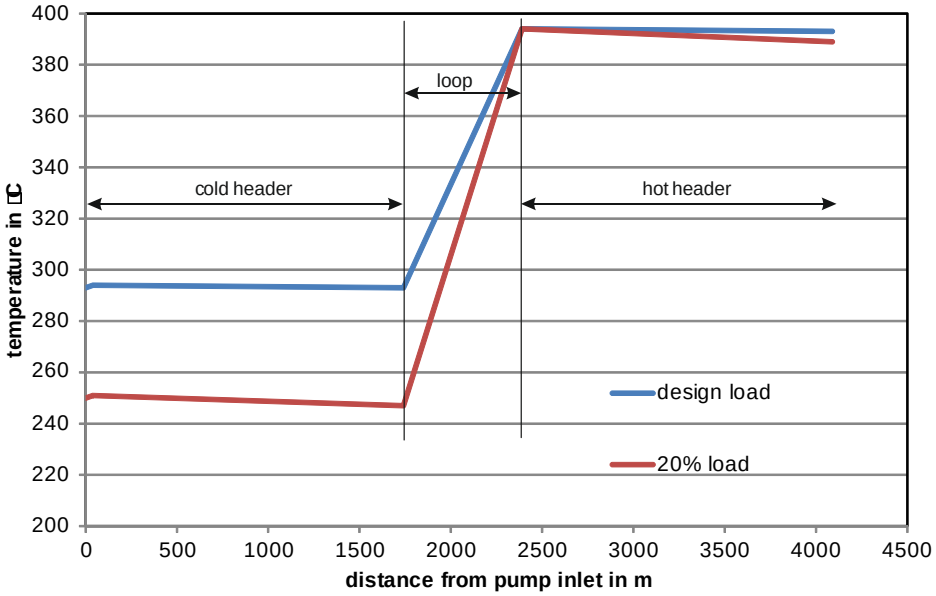

Figure C-18: Temperature profile from pump inlet to solar field outlet in a large parabolic trough plant for 2 load cases.

Heat gains

Heat gains for parabolic trough solar fields are mainly caused by the pressure loss and by trace heating elements if such elements exist in the plant considered.

$$\sum \dot{Q}_{\text{gain}} = \dot{Q}_{\Delta p} + \dot{Q}_{\text{TH}} \tag{C.38}$$

Thermal gain from pumps

Main solar field pumps are large electricity consumers and as other technical equipment they are not perfect. Only a certain fraction of the electricity used by them is actually transferred into pressure increase. About 20 % (the actual value depends on the pump efficiency) of the electric consumption is dissipated at the pump and mainly increases the HTF temperature between pump inlet and outlet.

$$\dot{Q}_{\text{pump}} = (1 - \eta_P)\, P_{\text{el,P}} \;=\; \dot{m}_{\text{HTF}}\, c_{\text{HTF}} \left(T_{pump,out} - T_{pump,in}\right) \tag{C.39}$$

This is the thermal power which is directly supplied to the HTF at the pumps and this will lead to a slightly increased inlet temperature.

The pressure loss of the solar field means that this energy is dissipated into heat too and must be considered in the energy balance since the electric power needed might be in the range of 2 % of the plants gross electrical annual output.

$$\dot{Q}_{\Delta \text{p}} = \Delta p\; 10^5 \frac{\text{Pa}}{\text{bar}} \frac{\dot{m}_{\text{HTF}}}{\rho_{HTF}} \tag{C.40}$$

This is an additional heat input for the solar field (see Eq. (C.41)).

Balance equation for the whole solar field

With all the effects explained in the section above Eq. (C.4) becomes:

$$\dot{Q}_{\text{steady}}^{\text{SF}} = \left[n_{\text{loops}} \left(IAM\ \eta_{\text{opt},0}\ \eta_{\text{shad}}\ \eta_{\text{clean}}\ f_{\text{focA}}\ A_{\text{nom,loop}}\ G_{\text{pr}} - n_{\text{Coll, loop}}\ n_{\text{Abs, Coll}}\ l_{\text{Abs}}\ \dot{q}_{\text{loss,rec}} - l_{\text{pipe,loop}}\ \dot{q}_{\text{loss,pipe}} \right) - l_{\text{header}}\ \dot{q}_{\text{loss,head}} + \dot{Q}_{\Delta p} \right] \quad \text{(C.41)}$$

C.2.1.4. Pressure loss

The flow of HTF through receivers, headers, heat exchangers, pipe fittings and valves etc. leads to losses of flow energy due to irreversible processes which can be denoted as pressure losses. These losses may occur by friction, vortex shedding and secondary flow, whereas flow energy is always converted into heat. The solar field model must be capable to calculate these losses since main HTF pumps have to provide this pressure difference (plus the pressure difference caused by the solar steam generators and the storage heat exchangers). During detailed engineering of a CSP plant, dimensioning of piping and headers follows a techno-economic optimization since there is always a trade-off between minimal pressure loss and minimal HTF and steel masses.

There are two different modeling approaches:

1. Calculation or estimation of pressure losses for design conditions and scaling with solar field thermal load.
2. Individual pressure loss calculation for every time instance.

The first approach is often used in annual performance models. Pressure drop calculation for pipes, fittings, valves, etc. can be found in textbooks. For the reference systems the nominal pressure drop is given in Appendix B. Pressure loss of single phase fluid systems is proportional to the square of fluid velocity.

$$\Delta \text{p} \sim v_{HTF}^2 \quad \text{(C.42)}$$

Therefore, a quadratic scaling law for pressure drop may be applied in part load conditions.

$$\Delta \text{p} = \Delta p_{\text{nom}} \left(\frac{\dot{V}_{\text{HTF}}}{\dot{V}_{\text{HTF,nom}}} \right)^2 = \Delta p_{\text{nom}} \left(\frac{\dot{m}_{\text{HTF}} \cdot \rho_{\text{HTF,nom}}}{\rho_{\text{HTF}} \cdot \dot{m}_{\text{HTF,nom}}} \right)^2 \quad \text{(C.43)}$$

C.2.1.5. Auxiliary electrical consumption

The solar field needs electrical power for pumping, control, etc. which may be divided into two fractions: One fraction depends on load and/or solar field state and ambient conditions and the second one is constant. The auxiliary demand of the solar field will be different for periods with and without irradiance but in general, even during times without usable irradiance, there will be a certain electricity demand.

$$P_{\mathrm{aux}}^{\mathrm{SF}} = P_{\mathrm{aux,var}}^{\mathrm{SF}} + P_{\mathrm{aux,fix}}^{\mathrm{SF}} \tag{C.44}$$

In addition to the pumping power to overcome the pressure losses, the solar field has typically further electrical consumers:

- drives used to turn the parabolic troughs and for tracking the sun
- instrumentation and control devices
- trace heating of pipes and vessels which need freeze protection

The bullet points above show that the electrical consumers of a solar field may be divided into several groups:

- Equipment with load dependent consumption (e.g. main HTF pumps)
- Equipment with almost constant consumption when the solar field is in operation (e.g. tracking drives, auxiliary consumers of the HTF system)
- Equipment with almost constant consumption when the solar field is out of operation (e.g. those parts of I&C which are used for continuous monitoring)
- Equipment which is only used under special conditions (e.g. trace heating, freeze protection pumps or solar field recirculation pumps)

Therefore, the electric power consumption of the solar field depends on the status of the solar field itself[2]:

$$P_{\mathrm{el,on}}^{\mathrm{SF}} = P_{\mathrm{pump,nom}} \left(\frac{\dot{m}_{\mathrm{HTF}} \cdot \rho_{\mathrm{HTF,nom}}}{\rho_{\mathrm{HTF}} \cdot \dot{m}_{\mathrm{HTF,nom}}} \right)^2 + P_{\mathrm{fix,on}}^{\mathrm{SF}} \tag{C.45}$$

With the base load auxiliary consumption of the solar field when the solar is in operation: $P_{\mathrm{BL,on}}^{\mathrm{SF}}$.
The nominal power of the main HTF pumps can be calculated from the nominal pressure loss.

$$P_{\mathrm{pump,nom}} = \frac{\Delta p_{nom}\, \dot{V}_{HTF,nom}}{\eta_P} = \frac{\Delta p_{nom}\, \dot{m}_{HTF,nom}}{\eta_P\, \rho_{HTF,nom}} \tag{C.46}$$

[2] Update is in preparation taking into account the specific part-load behavior of the pumps

If the solar field is not in operation the power is reduced to the constant offline auxiliary consumption and eventually the power consumption of recirculation pumps:

$$P_{\mathrm{el,off}}^{\mathrm{SF}} = P_{\mathrm{fix,off}}^{\mathrm{SF}} + P_{\mathrm{reci}} \quad \text{(C.47)}$$

The mean electrical own consumption of one collector drive for a parabolic trough collector of about 150 m length and 5.77 m aperture width is in the range of 23 W when the collector is tracking and in the range of 3 W in stow position. These values are valid for collector equipped with hydraulic drives with individual drives for each collector. The actual instantaneous electrical power of these hydraulic pumps is higher but they are only operated temporarily.

C.2.1.6. Losses caused by operational limits

In a real CSP plant most of the installed technical equipment has well defined limits for operation and sometimes the limit of one single part restricts the output of the whole plant. These limits are mainly:

- Minimum operation limit: Many parts of the solar field (receivers, pumps, heat exchangers, etc.) have a minimum fluid flow in order to maintain stable working conditions, thus not every sun beam can be used for plant operation.
- Maximum operation limit: The same is valid for maximum flows, temperature limits etc.
- The thermal storage has a limited capacity and during sunny summer days it might be totally charged prior to sunset.
- Maximum wind velocity (or rather gusts): Collectors and heliostats sustain a certain upper wind speed for operation (provided by suppliers). Above that wind speed they must be turned into stow position in order to avoid damages. Time periods with high irradiation and high wind velocity can thus not be accounted for production.
- Some parts of the plant (particularly heat exchangers and steam turbine) have restrictions for heating-up or cooling down.

Above mentioned limits may reduce the actual output of the solar field and a fraction of the available solar energy cannot be utilized. In annual performance models it is important to define and report these limits in order to obtain comparable results. The solar field model must provide interface variables as output specifying the minimum and maximum HTF mass flow rate. These values might be constant or variable from time step to step, depending on the actual plant design.
The fraction of the theoretical solar field heat output which could be produced but actually cannot be used due to operational limits is called defocussed energy. The annual sum of defocussed energy should be reported since it can be used to evaluate the design of a CSP plant.

C.2.1.7. Transient effects

All models in chapter C.2 are valid for steady state operation and the overall modeling approach is also a steady state model with constant input and output for individual time steps. Nevertheless the goal is to predict the annual output of power plants with large fluctuations of the main input parameter DNI, which may be considered as the driving "fuel". The steady state model does not consider that startup and load variation is not instantaneous but requires certain time. Equation (C.1) contains an additional part to consider transient effects $\dot{Q}_{\mathrm{trans}}$.

The major and dominating transient effect of the solar field is its thermal inertia. The yield calculation is influenced by thermal effects which are initiated during plant start-up and shut down and during cloud effects by which the solar energy input changes rapidly. The change of energy input during a clear sky day due to the normal increase and decrease of the DNI levels and due to the changing incidence angle can be seen as subordinated to the aforementioned causes. Changes of operating states are slow; the operating states can be considered as a sequence of stationary conditions.

Parabolic trough solar fields contain large amounts of HTF (typically more than 3000 tons for a 100 MW_e plant with storage) and steel pipes with direct contact to HTF (this steel mass is in the same order of magnitude as for HTF mass). During the night and hours without DNI, this solar field inventory cools down and must be heated up again to nominal operating conditions before the next operation phase can begin. During this period the solar field does not deliver any "useful" heat which could be used to charge the storage or to operate the power block. Instead the collected heat is mainly utilized to increase the temperature of the solar field itself. On the other hand thermal inertia of the solar field may be used to operate the power block for a certain time period even after the irradiation disappears. Typically the heat which has to be put into the system during startup is higher than the heat which can be recovered after sunset since the solar field will cool down during the whole night and the heat stored in HTF and piping can only be utilized down to a certain temperature. Sometimes it is even not desired to utilize this heat but rather use it to keep the temperature in the system at a higher level in order to reduce startup time in the next morning. The actual practice depends on the design of the plant and the operating concept.

Clouds may shade parts of the solar field or even the whole solar field for a short time period, causing fluctuations in heat output, either temperature or mass flow fluctuations or both. In extreme situations this might be so pronounced that the power block cannot be operated though the mean DNI over a time period of one hour would be sufficient.

The steady state thermal output of the solar field may be reduced by transient effects, thus the solar field net thermal energy which can be delivered to power block and/or thermal storage in a time step is:

$$Q^{SF} = \left(\dot{Q}^{SF}_{steady} \cdot \Delta t - Q_{\mathrm{heatup}}\right) \cdot \xi_{\mathrm{cloud}} \qquad \text{(C.48)}$$

Equation (C.48) is written in terms of thermal energy rather than thermal power since heating up and net heat production may occur in the same time step but not simultaneously. The factor ξ_{cloud} is

introduced to account for losses caused by clouds. Its value is between 0 and 1.0 and may vary from time step to time step. Currently it should be set to 1.0, neglecting losses caused by transients due to clouds because there is no validated model available. Once appropriate models are available the factor may be calculated and used to correct the solar field output.
The heat required for startup or provided by the HTF and steel mass during cool down may be calculated from:

$$Q^{\mathrm{SF}}_{\mathrm{inertia,ideal}} = \left(m_{HTF} \cdot c_{HTF} + m_{pipe} \cdot c_{\mathrm{pipe}}\right)\left(\bar{T}_{HTF} - \bar{T}_{HTF,t-\Delta \mathrm{t}}\right) \quad \text{(C.49)}$$

This equation accounts for the heat capacity of HTF inventory and the heat capacity of the piping in contact with the fluid. The latter value can be found by calculating the steel mass present in the solar field and might therefore be difficult to determine; thus another option would be to use solely the HTF heat capacity and multiply it by a factor $b_h > 1$.

$$Q^{\mathrm{SF}}_{\mathrm{inertia,ideal}} = b_h \cdot m_{\mathrm{HTF}} \cdot c_{\mathrm{HTF}} \cdot \left(\bar{T}_{HTF} - \bar{T}_{HTF,t-\Delta t}\right) \quad \text{(C.50)}$$

The factor b_{h} = 1.2 to 1.5 for a typical parabolic trough plant with 50 or 100 MW nominal electrical output.

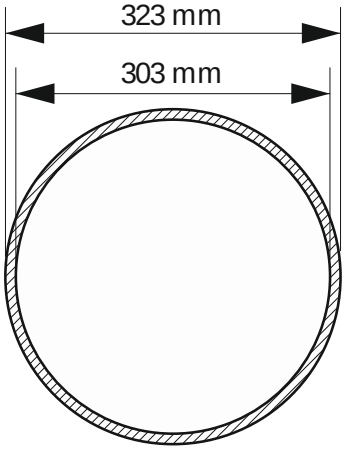

$$\boldsymbol{\vartheta_{\mathrm{HTF}} = 350°C}$$

$$\boldsymbol{\rho_{\mathrm{HTF}} = 770\frac{kg}{m^3}, \quad c_{\mathrm{HTF}} = 2430\ \frac{J}{kg\ K}}$$

$$\boldsymbol{\rho_{\mathrm{pipe}} = 7900\frac{kg}{m^3}, \quad c_{\mathrm{pipe}} = 550\ \frac{J}{kg\ K}}$$

$$\boldsymbol{m_{\mathrm{HTF}}c_{\mathrm{HTF}} = 134919\frac{J}{K}}, \qquad \boldsymbol{m_{\mathrm{pipe}}c_{\mathrm{pipe}} = 42725\frac{J}{K}}$$

Figure C-19: Example for the relation of fluid and steel heat capacity of a 12” header pipe filled with thermal oil

[Hirsch 2012] proposed the use of an additional startup factor >1 to account for heat required or lost during plant startup, which would otherwise not be considered in ideal energy calculation. The startup factor accounts e.g. for heating up other parts of the plant (in addition to HTF and piping) or for ramp up limits of some parts of the plant causing additional heat losses. The startup correction factor ψ_{SU} might also be used to adapt simulated start up times to measured start up times if such information is available.

$$Q_{\text{inertia}}^{\text{SF}} = \psi_{\text{SU}}\left(m_{HTF} \cdot c_{HTF} + m_{pipe} \cdot c_{pipe}\right)\left(\bar{T}_{HTF} - \bar{T}_{HTF,t-\Delta t}\right) \quad \text{(C.51)}$$

[Hirsch 2012] proposed first estimates for startup correction factors of 1.3 for good (clear sky) conditions, 1.5 for mean (some small cloud events taking place during the start-up) and 1.7 for bad (strong clouds that lead to an interruption of the startup process) irradiation conditions.

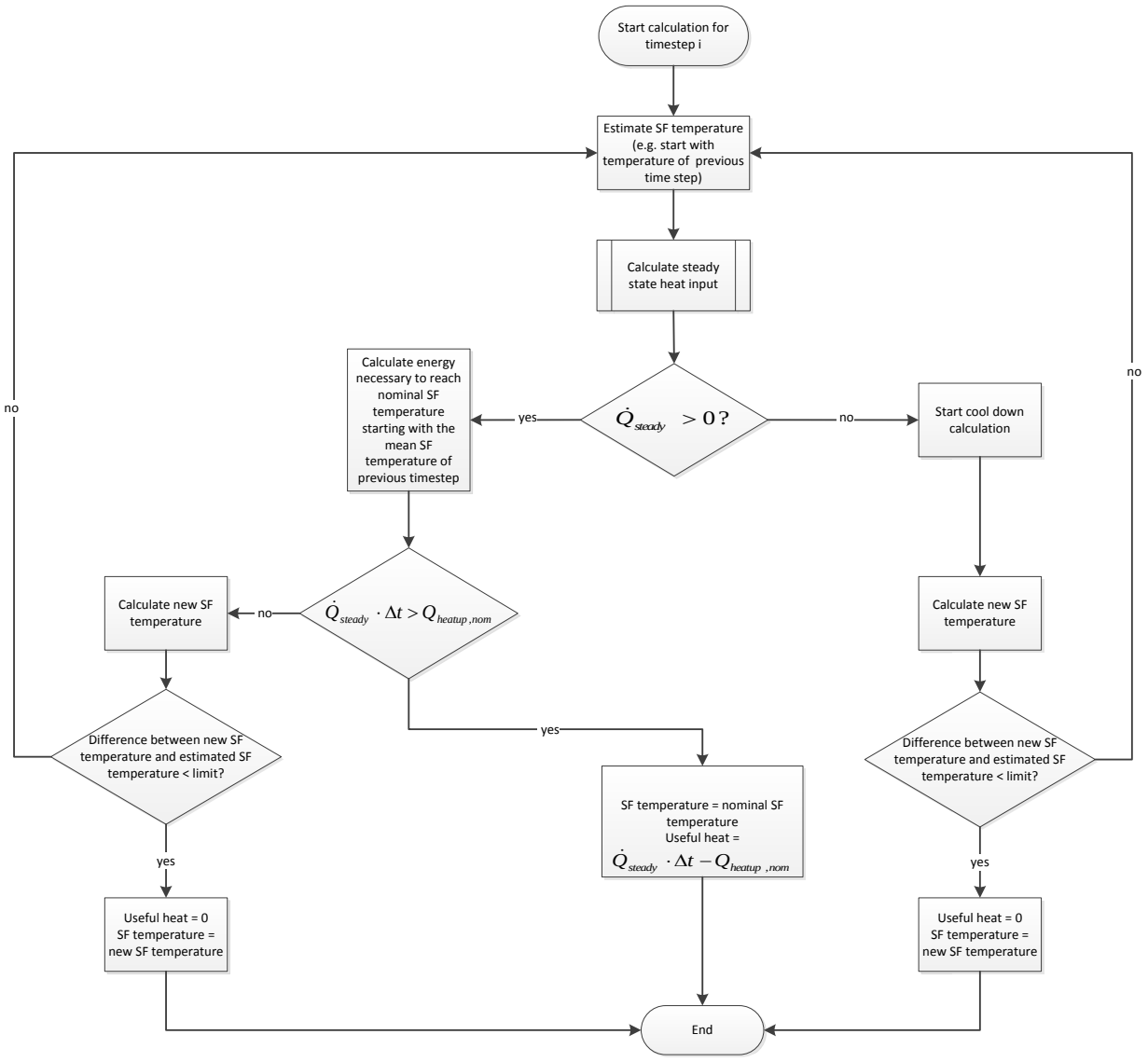

Figure C-20: Flow chart for the solar field performance calculation for a single time step

Nominal solar field outlet temperature will not always be reached at the end of an individual time step but rather in between. For large time steps like 1 hour it would then be necessary to split the time steps in order to consider different operation modes. For the recommended time resolution of 10 minutes this is not necessary because the impact is quite small.

Similar to the heat up losses in the morning the solar field contains a lot of thermal energy after sunset which might be used to extend the power production. The total HTF inventory of hot headers and hot runners is at solar field outlet temperature and might be used to operate the power block for a certain time. On the other hand, this utilization would reduce the mean solar field temperature at the beginning of the night operation. The solar field cool down during night starts at a lower level and the HTF temperature reached on the next day will be lower compared to the case without utilization of the remaining heat of the hot headers and runners. Actually it will be a decision of the plant operator, but in this handbook the utilization of hot header and runner inventory for electricity production after sunset is not modelled.
Instead the solar field will be considered to cool down starting at almost nominal temperatures and the model should be able to calculate the solar field temperature decrease in order to decide whether freeze protection will be necessary or not and to obtain the appropriate temperature for the startup simulation in the next morning. If the steady state thermal power calculated by equation (C.41) is negative, the solar field will cool down during the current time step. The cool down heat can be calculated by multiplying the steady state thermal power by the time increment.

$$Q_{\text{cooldown}} = \dot{Q}_{steady}^{SF} \cdot \Delta t = \psi_{\text{CD}}\left(m_{HTF} \cdot c_{HTF} + m_{pipe} \cdot c_{pipe}\right)\left(\overline{T}_{HTF} - \overline{T}_{HTF,t-\Delta t}\right) \qquad \text{(C.52)}$$

The right hand side of this equation is then used to calculate the new HTF temperature at the end of the current time step. Analogous to the imperfect startup correction factor an imperfect cooldown correction factor is used in Equation (C.52).

C.2.1.8. Night operation and freeze protection

Thermal losses during periods without direct solar irradiation cause a temperature decrease in the whole system which would tend to cool down to ambient temperature during long downtimes if no measures are taken to keep the temperature above a certain value. The pour point of DPO/BP is at 12 °C but actually operators will try to have a threshold temperature which is well above this value in order to ensure that even in case of “cold spots” no solidification occurs. Thus active freeze protection measures might be started at about 50 or 60 °C or even higher.
There are different options for freeze protection:

1. Utilization of internal thermal energy from the system (homogenization by recirculation, heat from storage, tanks, etc.)
2. Utilization of external energy sources (fossil fuel heater, electricity from grid)

The actual source depends on specific conditions for individual plants:

- Is there a thermal storage present at this plant?
- Are fossil fuel and a heater available?
- Is the plant equipped with electrical heaters?

In case of utilization of internal thermal energy for freeze protection, the reduction of internal energy must be considered in the overall energy balance of the plant and therefore the plant starts from a

lower energy level in the next morning. In case fossil fuel or electricity is utilized the relevant amount must be summed up and considered in the financial model as part of the operating costs.
Provided that the heat loss equations for receivers, piping and headers are valid down to anti-freeze temperature, heat losses of the solar field may be calculated from:

$$\dot{Q}_{\mathrm{AF}} = n_{\mathrm{loops}} \cdot \left[n_{\mathrm{Coll,loop}}\, n_{\mathrm{Abs,Coll}}\, l_{Abs}\, \dot{q}_{\mathrm{loss,rec}} + l_{\mathrm{pipe,loop}}\, \dot{q}_{\mathrm{loss,pipe}} (\vartheta_{\mathrm{AF}} - \vartheta_{\mathrm{amb}}) \right] + l_{\mathrm{head}}\, \dot{q}_{\mathrm{loss,head}}\, (\vartheta_{\mathrm{AF}} - \vartheta_{\mathrm{amb}}) - P_{\mathrm{reci}} \qquad \text{(C.53)}$$

This is again equation (C.41) without heat input from the sun and without thermal losses of other HTF equipment, which should be close to zero in this operation mode. Although the freeze protection model assumes that the HTF will be circulated all the time with low mass flow rate, this might not be the case in all parabolic trough plants. Instead the circulation or freeze protection pump is only used occasionally. In this case heat input from the pump as well as electrical consumption by the pump is not constant but will be only present during singular time steps.
All heat losses depend on the solar field temperature, which requires an iterative calculation as shown in Figure C-20. One option to limit the computational effort is to utilize the solar field temperature of the previous time step, at least for some operation modes. Figure C-21 shows the impact of different simplifications on the calculated mean solar field temperature for cooling down over 12 hours. This figure indicates that one hour time steps and the utilization of nominal HTF mass and heat capacity are acceptable for the simulation of solar field cool down in annual performance calculations. In terms of energy losses the difference between the simplest approach (blue line) and the most complex approach is less than 1 % when comparing the sum of heat losses for 12 hours.

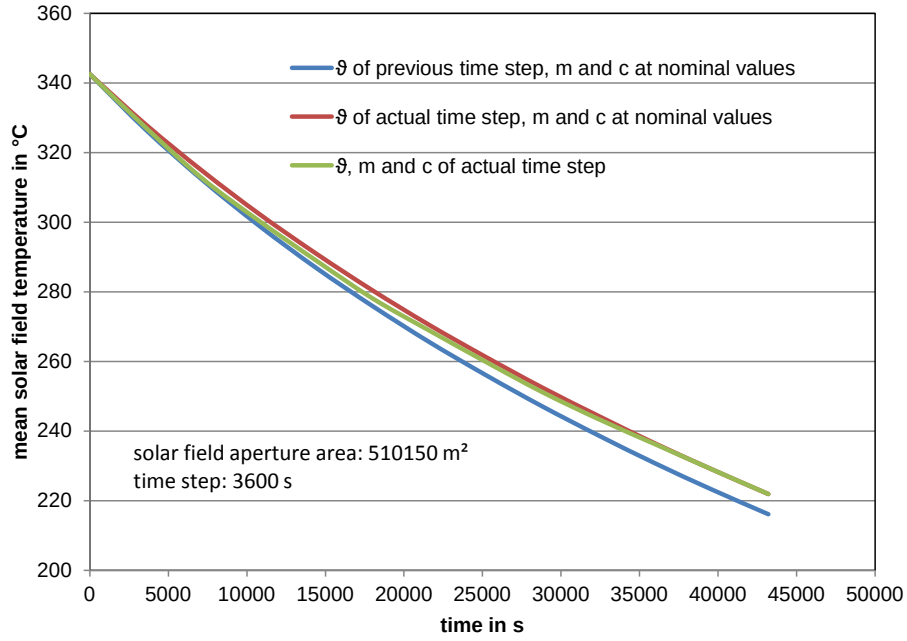

Figure C-21: Calculated cool down of a large solar field with different assumptions for temperature, HTF mass and specific heat capacity

From Figure C-22 it is obvious that the error becomes smaller when switching to 10 minutes time steps as recommended.

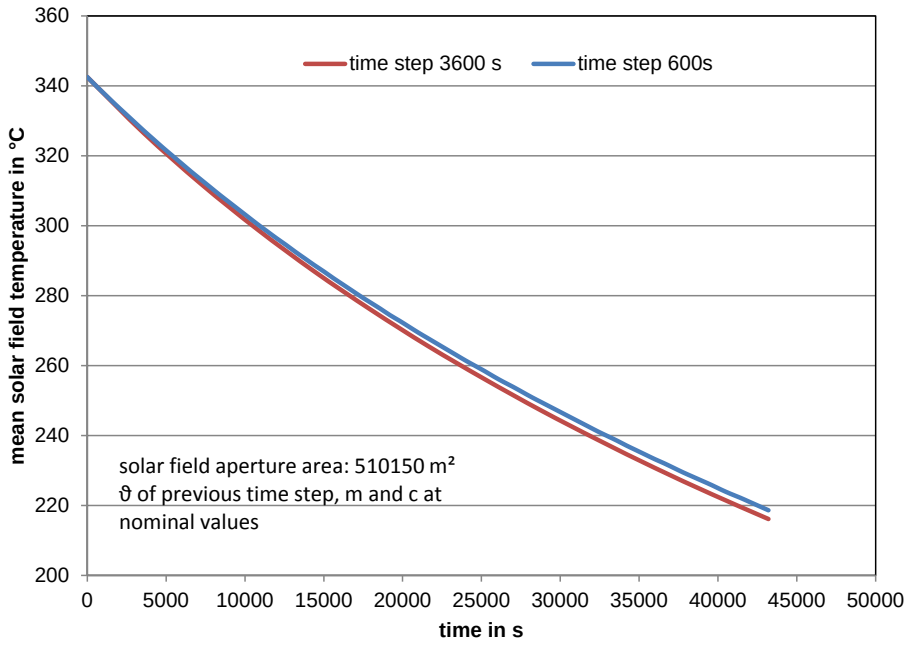

Figure C-22: Calculated cool down of a large solar field with different time steps

C.2.1.9. Interface variables

For the annual performance simulation of the whole CSP plant several interface variables as defined in Appendix A must be calculated.

From the solar field's view point inlet temperature, inlet enthalpy and outlet pressure are input variables. Outlet temperature, outlet enthalpy, inlet pressure, HTF mass flow rate, net thermal power and auxiliary consumption are output variables.

For the calculation of output interface variables the current status of the solar field must be determined as shown in Figure C-20.

If the solar field can deliver net thermal power the following table is valid:

$$T_{\text{out}}^{\text{SF}} = T_{\text{nom}}^{\text{SF}} \quad [3] \tag{C.54}$$

$$h_{\text{out}}^{\text{SF}} = h_{\text{nom}}^{\text{SF}} \tag{C.55}$$

$\dot{Q}^{SF}$ from equation (C.41) (C.56)

[3] Must not be neccessarily nominal SF outlet temperature. The OS should at least have the option request a SF temperature for the time step and the SF must try to deliver this temperature

$$\dot{m}^{\mathrm{SF}} = \frac{\dot{Q}^{\mathrm{SF}}}{\left(h_{\mathrm{out}}^{\mathrm{SF}} - h_{\mathrm{in}}^{\mathrm{SF}}\right)} \tag{C.57}$$

$$\mathrm{p}_{in}^{SF} = p_{out}^{SF} - \Delta p_{\mathrm{nom}} \left(\frac{\dot{m}_{HTF} \cdot \rho_{HTF,nom}}{\dot{m}_{HTF,nom} \cdot \rho_{HTF}} \right)^2 \tag{C.58}$$

$$\mathrm{P}_{aux}^{SF} = P_{\mathrm{pump,nom}} \left(\frac{\dot{m}_{HTF} \cdot \rho_{HTF,nom}}{\dot{m}_{HTF,nom} \cdot \rho_{HTF}} \right)^2 + P_{fix,on}^{SF} \tag{C.59}$$

If the solar field cannot deliver net thermal power it is in recirculation mode with:

$$T_{out}^{SF} = T_{in}^{SF} \tag{C.60}$$

$$h_{out}^{SF} = h_{in}^{SF} \tag{C.61}$$

$$\dot{Q}^{SF} = 0 \tag{C.62}$$

$$\dot{m}^{SF} = 0 \tag{C.63}$$

$$\mathrm{p}_{in}^{SF} = 0 \tag{C.64}$$

$$P_{aux}^{SF} = P_{\mathrm{reci}} + P_{fix,off}^{SF} \tag{C.65}$$

C.2.1.10. Plausibility checks

The following checks should be done for a model, in order to identify crude errors:

- Are the associated values for optical efficiency and aperture areas (and eventually specific costs) used?
- Is the IAM function (for parabolic troughs) beneath the cosine function (see Figure C-8)?
- Is the approximation for receiver thermal losses valid and physically reasonable for the whole temperature range?
- Check the time code used in the meteorological dataset and take care to use the same time in the model
- Check the definition of the time stamp used in the meteorological data file and use appropriate time to calculate mean sun position for the time instance.
- Plot diagrams of typical solar days and analyze course of power generation in order to identify failures in the system behavior

C.2.2. Parabolic trough field with two-phase heat transfer fluid (place holder)

C.2.3. Linear Fresnel field with single phase heat transfer fluid (place holder)

C.2.4. Linear Fresnel field with two-phase heat transfer fluid (place holder)

C.3. Solar towers

This chapter will be available by beginning of February 2017.

C.4. Symbols

C.4.1. Symbols used in chapter C.2

Symbol	Description	Unit
A_{net}	Net aperture area	m²
$A_{\mathrm{nom,reduced}}$	Reduced nominal aperture area (due to missing mirrors etc.)	m²
$A_{\mathrm{nom}*}$	Nominal aperture area without receiver area	m²
$A_{\mathrm{nom,loop}}$	Nominal aperture area of one loop	m²
A_{rec}	Net receiver area	m²
A^{SF}	Aperture area of the solar field	m²
a_{k}	Coefficient of the IAM equation	
a_{shad}	Additional shaded fraction of the solar field	-
b_{h}	Factor considering the piping mass and heat capacity in relation to the HTF mass and heat capacity	-
b_{i}	Coefficient of receiver heat loss equation	
c_{HTF}	Specific heat capacity of HTF	kJ/kg/K
c_{pipe}	Specific heat capacity of pipe material	kJ/kg/K
d_{col}	Axial distance between collectors in a row	m
d_{row}	Row distance in the solar field	m
F'	Heat loss factor accounting for the difference between absorber temperature and bulk HTF temperature	-
f	Collector focal length	m
f_{corr}	Correction factor to account for the non-linearity of receiver heat losses in temperature	-
f_{focA}	Focusing factor	-
G_{bn}	Beam irradiance	W/m²
G_{d}	Diffuse irradiance	W/m²
G_{Pr}	Projected direct irradiance	W/m²
K	Incidence angle modifier	-
K'	Incidence angle modifier including cosine of incidence angle	-
l_{col}	Collector length	m
$l_{f,aver}$	Average distance between reflector and receiver	m
l_{pipe}	Piping length	m
$l_{pipe,loop}$	Total piping length of one loop (excluding receivers)	m
l_{head}	header length	m
$h_{\mathrm{in}}^{\mathrm{SF}}$	Inlet enthalpy of SF	kJ/kg
$h_{\mathrm{out}}^{\mathrm{SF}}$	Outlet enthalpy of SF	kJ/kg
l_{rec}	Receiver length	m

m_{HTF}	Total mass of HTF	kg
m_{pipe}	Total mass of pipes (loop piping and headers)	kg
$\dot{m}_{\mathrm{HTF}}$	HTF mass flow rate	kg/s
$n_{col,loop}$	Number of collectors per loop	-
$n_{\mathrm{col,row}}$	Number of collectors in one row	-
$n_{rec,coll}$	Number of receivers per collector	-
n_{row}	Total number of rows in the solar field	-
$n_{\mathrm{row,unshad}}$	Number of rows which are not affected by shading	-
$P_{\mathrm{aux}}^{\mathrm{SF}}$	Total auxiliary power consumption of SF	W
$P_{\mathrm{aux,fix}}^{\mathrm{SF}}$	Constant auxiliary power consumption of SF	W
$P_{\mathrm{aux,var}}^{\mathrm{SF}}$	Variable (load dependent) auxiliary power consumption of SF	W
$P_{\mathrm{el,P}}$	Electrical power consumption of solar field pumps	W
$P_{el,on}^{SF}$	Total online electric power consumption of solar field	W
$P_{\mathrm{fix,off}}^{\mathrm{SF}}$	Constant part of the offline electric power consumption of solar field	W
$P_{\mathrm{fix,on}}^{\mathrm{SF}}$	Constant part of the online electric power consumption of solar field	W
$P_{el,off}^{SF}$	Total offline electric power consumption of solar field	W
P_{reci}	Power consumption of the solar field recirculation pump (pump used for circulating the HTF when the solar field is in start-up or anti-freeze mode)	W
$P_{\mathrm{pump,nom}}$	Nominal power of main HTF pumps	W
$p_{\mathrm{in}}^{\mathrm{SF}}$	Pressure at SF inlet	bar
$p_{\mathrm{out}}^{\mathrm{SF}}$	Pressure at SF outlet	bar
Q_{cooldown}	Cool down heat within a time interval	J
$Q_{\mathrm{inertia}}^{\mathrm{SF}}$	Heat used for solar field heat up within a time interval	J
Q^{SF}	Total delivered heat by the solar field within a time interval	J
$\dot{Q}_{\mathrm{AF}}$	Anti-freeze thermal power	W
$\dot{Q}_{\mathrm{TH}}$	Thermal power from trace heating	W
$\dot{Q}_{\mathrm{abs}}$	Absorbed thermal power	W
$\dot{Q}_{\mathrm{abs,0}}$	Nominal absorbed thermal power	W
$\dot{Q}_{\mathrm{ext}}$	Heat gain from external sources (e.g. solar field pumps or trace heating	W
$\dot{Q}_{loop,steady}$	Thermal power delivered by one loop calculated without considering transient effects	W
$\dot{Q}_{\mathrm{loss}}$	Heat losses	W
$\dot{Q}_{loss,\mathrm{cold}\ head}$	Heat loss of cold header	W
$\dot{Q}_{\mathrm{loss,head}}$	Header heat losses	W
$\dot{Q}_{loss,\mathrm{hot}\ head}$	Heat loss of hot header	W

$\dot{Q}_{\mathrm{loss,loop}}$	Total heat loss of a single loop	W
$\dot{Q}_{\mathrm{loss,rec}}$	Receiver heat losses	W
$\dot{Q}_{\mathrm{loss,pipe}}$	Piping heat losses of solar field loops	W
$\dot{Q}_{\mathrm{pump}}$	Heat gain caused by HTF pumps	W
$\dot{Q}^{SF}$	Thermal power delivered by solar field	W
$\dot{Q}^{SF}_{steady}$	Thermal power delivered by solar field calculated without considering transient effects	W
$\dot{Q}_{\Delta \mathrm{p}}$	Thermal power input to the solar field due to friction losses of the HTF	W
$\dot{q}_{\mathrm{loss,corr}}$	Corrected specific receiver heat loss	W/m
$\dot{q}_{\mathrm{loss,head}}$	Specific header losses based on header length	W/m
$\dot{q}_{\mathrm{loss,head,A}}$	Specific header losses based on net aperture area	W/m²
$\dot{q}_{\mathrm{loss,pipe}}$	Specific piping heat losses based on pipe length	W/m
$\dot{q}_{\mathrm{loss,pipe,nom}}$	Specific piping heat losses based on pipe length for nominal solar field conditions	W/m
$\dot{q}_{\mathrm{loss,rec}}$	Specific receiver heat losses based on receiver length	W/m
T_{amb}	Ambient temperature	K
T_{HTF}	Bulk HTF temperature	K
$T^{\mathrm{SF}}_{\mathrm{in}}$	Solar field inlet temperature	K
$T_{\mathrm{loop,in}}$	Loop inlet temperature	K
$T_{\mathrm{loop,out}}$	Loop outlet temperature	K
$T^{\mathrm{SF}}_{\mathrm{out}}$	Solar field outlet temperature	K
$T_{\mathrm{pump,in}}$	HTF temperature at pump inlet	K
$T_{\mathrm{pump,out}}$	HTF temperature at pump outlet	K
$\bar{T}_{\mathrm{HTF}}$	Local mean HTF temperature of the current time step	K
$\bar{T}_{HTF,t-\Delta t}$	Local mean HTF temperature of the previous time step	K
$\dot{V}_{\mathrm{HTF,nom}}$	Nominal HTF volume flow rate	m³/s
v_{HTF}	Velocity of heat transfer fluid	m/s
v_{wind}	Wind velocity	m/s
w_{col}	Collector aperture width	m
	Greek symbols	
α_{S}	Solar altitude angle	°
β_{A}	Collector axis tilt angle	°
γ_{A}	Collector axis azimuth angle	°
γ_{S}	Solar azimuth angle	°
$\Delta \mathrm{p}$	Pressure loss	bar
Δt	Time intervall	s
η_{abs}	Receiver tube absorptance	-

η_{atten}	Atmospheric attenuation efficiency	-
$\eta_{\mathrm{avail}}^{\mathrm{SF}}$	Solar field availability	-
η_{block}	Blocking efficiency	-
η_{clean}	Cleanliness factor	-
η_{phi}	Incidence angle efficiency including all losses caused by non-perpendicular sun rays into the aperture plane	-
η_{endloss}	End loss efficiency	-
η_{refclean}	Reflector cleanliness	-
η_{inter}	Intercept factor	-
η_{opt}	Optical efficiency	-
$\eta_{\mathrm{opt,0}}$	Clean optical efficiency at incidence angle of zero	-
$\eta_{opt,0,soiled}$	Optical efficiency under soiled conditions	-
η_{P}	Pump efficiency	-
η_{phi}	Incidence angle efficiency including all losses caused by non-perpendicular sun rays into the aperture plane	-
η_{recclean}	Receiver cleanliness	-
$\eta_{\mathrm{refl,0}}$	Clean reflector efficiency	-
η_{shad}	Shading efficiency	-
$\eta_{\mathrm{shad,row}}$	Row-to-row shading efficiency	-
η_{trans}	Transmission through receiver glass cover	-
θ_{i}	Incidence angle	°
ϑ_{abs}	Absorber temperature	°C
ϑ_{amb}	Ambient temperature	°C
ϑ_{HTF}	HTF bulk temperature	°C
ψ_{CD}	Correction factor to account for non-ideal cooldown	-
ψ_{SU}	Correction factor to account for non-ideal startup	-
ρ_{HTF}	Density of heat transfer fluid	kg/m³
ρ_{track}	Collector track angle	°
ξ_{cloud}	Factor to account for reduced SF output due to transients caused by clouds	-
	Subscripts, Superscripts, Abreviations	
BP	Biphenyl	
DPO	Diphenyl oxide	
HTF	Heat transfer fluid	
nom	nominal	
SF	Solar field	

C.5. References

[Burkholder 2009] F. Burkholder and C. Kutscher: Heat Loss Testing of Schott's 2008 PTR70 Parabolic Trough Receiver, Technical Report NREL/TP-550-45633, May 2009

[Dersch 2012] J. Dersch J, K. Hennecke, V. Quaschning : Free Greenius – New Options and Availability, Proceedings of the SolarPACES 2012 Conference, 11.-14. September 2012, Marrakech, Morocco

[Duffie 1991] J.A. Duffie, W.A. Beckman: Solar Engineering of Thermal Processes, 2nd ed., John Wiley & Sons, New York, 1991

[Forristall 2003] R. Forristall, Heat Transfer Analysis and Modeling of a Parabolic Trough Solar Receiver Implemented in Engineering Equation Solver, National Renewable Energy Laboratory Technical Report, NREL/TP-550-34169, 2003. Available electronically from http://www.nrel.gov/csp/troughnet/pdfs/34169.pdf

[Herrmann 2004] Herrmann U., Graeter F., Nava P. "Performance of the SKAL-ET collector loop at KJC Operating Company" SolarPaces Symposium, Mexico, October 6-8, 2004

[Hirsch 2012] Hirsch T., Feldhoff F., Schenk H.: Start-Up Modeling for Annual CSP Yield Calculations. Journal of Solar Energy Engineering, Vol. 134, August 2012

[Janotte 2012] Janotte, Nicole: Requirements for Representative Acceptance Tests for the Prediction of the Annual Yield of Parabolic Trough Solar Fields. Dissertation, RWTH Aachen, 2012

[Lüpfert 2004] E. Lüpfert, U. Herrmann, H. Price, E. Zarza, R. Kistner: Towards standard performance analysis for parabolic trough collector fields. SolarPaces Symposium, Mexico, October 6-8, 2004

[Pernpeintner 2012] J. Pernpeintner: Measurement of Parabolic Trough Receiver Thermal Loss Power and Relative Optical Efficiency under Solar Simulator Light, Test Report DLR QUARZ, 2012, Available electronically from http://www.dlr.de/sf/Portaldata/73/Resources/dokumente/qualifizierung/quarz/testberichte/DLR-Quarz-Receiver-1207_Schott_R3.pdf

[Riffelmann 2011] K.J. Riffelmann, D. Graf, P. Nava: Suitable Solar Filed Layouts for the Ultimate Trough® Collector SolarPaces Symposium, Granada, Spain, 20.-23. Sept. 2011

[Riffelmann 2014] K.J. Riffelmann, T. Richert, P. Nava. A. Schweitzer: Ultimate Trough® – A significant step towards cost-competitive CSP. Energy Procedia 49 , pp.1831 – 1839, 2014

[Stine 1985] W.B. Stine and R.W. Harrigan: Solar energy fundamentals and design: with computer applications. New York, John Wiley & Sons, ISSN 0735-8210, 1985.

[Wilbert 2014] S. Wilbert: Determination of Circumsolar Radiation and its Effect on Concentrating Solar Power, Dissertation RWTH Aachen, Germany, 2014

[Wittmann 2012] M. Wittmann, F. Feldhoff, T. Hirsch: Determination of Correction Factors for Heat Losses at High Temperatures in Parabolic Trough Fields. International SolarPaces Conference, Marrakech, Morocco , September 11-14, 2012